Quantum Design

11578 Sorrento Valley Road
San Diego, CA 92121-1311
USA
http: / / www.quandsn.com /

Tel: 619.481.4400
800.289.6996
Fax: 619.481.7410
E-Mail: info@quandsn.com

Effects of Magnetic Field Uniformity on the Measurement of Superconducting Samples

Mike McElfresh and Shi Li of Purdue University
and
Ron Sager of Quantum Design

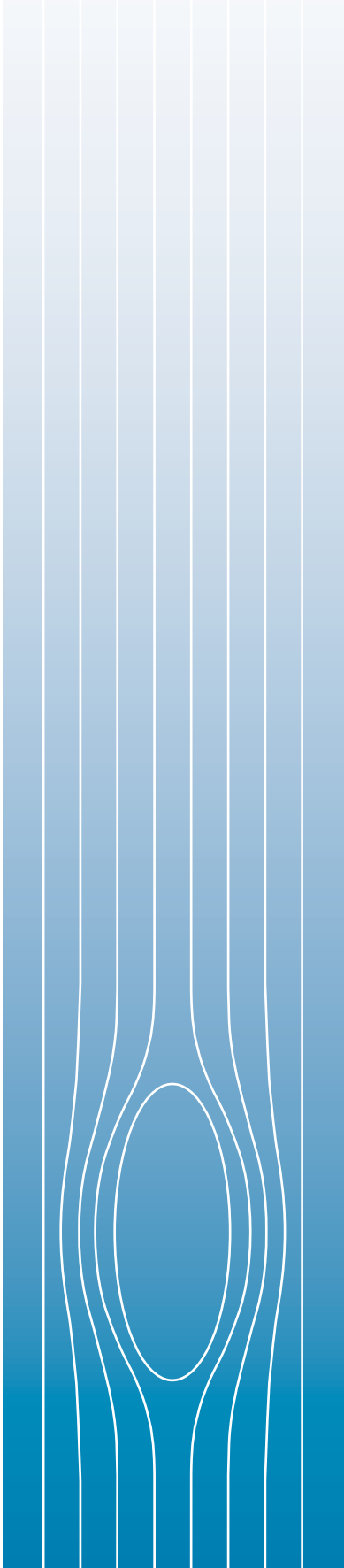

Table of Contents

A. Introduction

Since the discovery of the high-temperature superconductors, much has been learned about strong-pinning effects of magnetic flux in superconducting materials. These materials can display extreme magnetic hysteresis, and measurements on them can be affected dramatically if the magnetic history of the sample is altered or if the sample experiences even small variations in magnetic field during the measurement. As a result, during the last several years a variety of unexpected and unexplained phenomena have been reported for these materials. Sometimes these effects are real properties of the materials under investigation; in other cases the phenomena arise from an interaction between the measurement apparatus and the material itself.[1]

Researchers presently use a wide variety of both home-built and commercial equipment to characterize and study the magnetic properties of superconducting materials. While there are many types of magnetometers in use, we will focus on the subset of magnetometers that are generally used to measure the magnetic properties of small samples of materials. These "small sample magnetometers" use a variety of methods to measure the magnetic properties of the sample under study. We can classify these measurement methods into those that require motion of the sample, within or through a pickup coil (e.g., vibrating sample magnetometers, most SQUID magnetometers, extraction magnetometers), and those that measure a force or torque, in which case the sample is held stationary while the field is rotated or a gradient is applied (e.g., Faraday balance, Gouy method, torque magnetometers).

In systems in which the field is changed while holding the sample stationary, the sample is subjected to a time-varying magnetic field which affects the magnetic history of the sample. In this case the measurement results for superconductors must account for motion of vortices, eddy currents induced in the sample, and other dynamic effects which arise from the interaction of the time-varying field and the sample. Conversely, magnetometers which require that the sample be physically moved from one position to another can introduce similar effects because the magnetic field in such instruments is never exactly uniform. This study presents a systematic analysis that describes some of the effects that such magnetic field non-uniformity can produce when making magnetic measurements on superconducting materials. All of our measurements use a strong-pinning superconducting thin film with the film perpendicular to the magnetic field because this geometry is one of the most problematic configurations in which to make a magnetic measurement. This particular geometry will produce the largest demagnetization effects, thereby greatly amplifying the magnitude of the field non-uniformities experienced by the sample. This geometry is also appropriate for the high-T_c materials because their large crystalline anisotropy means that samples frequently have a very large effective aspect ratio, even for materials in bulk (polycrystalline) form.

In all magnetometers that move the sample during the measurement, the *raw data* is an output signal having an amplitude which is a function of either time, position, or both. The sample property to be measured (usually the magnetic moment of the sample) is then computed using some type of analytical model which is fit to the raw data from the measurement. However, the analysis method always makes assumptions about the magnetic behavior of the sample. For example, nearly all analysis methods assume that the magnetic moment of the sample:

1) approximates a magnetic dipole moment, and
2) the sign and value of this moment do not change during the measurement.

We will refer to these two assumptions as the *constant-dipole model*, and we will see that in the case of superconductors the second of these two assumptions is often not valid.

We want to emphasize here that the raw data produced by such a measurement is, in fact, the true magnetic response of the sample, and this signal contains important quantitative information about the magnetic nature of the sample. (This assumes, of course, that the measurement apparatus is operating correctly.) As we have stated, however, strong-pinning, superconducting samples do not necessarily behave as a magnetic dipole of constant magnitude, and in those cases the analysis algorithms which compute the sample moment can fail, producing unpredictable and misleading results. In other words, the indiscriminate use of a constant-dipole model, which is the normal analysis model provided with commercial magnetometer systems, can lead to completely erroneous interpretations of a sample's magnetic properties. This pitfall can be largely avoided if one takes the care to determine the actual measurement conditions and then models the magnetic behavior of the sample under the particular circumstances experienced during the measurement. This does require, however, that one construct an appropriate analysis method to extract the relevant information from the output signal, then apply that analysis method to the raw data from the measurement.

It is worth noting that the constant-dipole model can also fail for non-superconducting samples under certain circumstances. For example, the constant-dipole model will produce erroneous results when the magnetic moment

of the sample is not purely a dipole moment (but is a quadrupole moment or a sum of multipolar contributions, for example). This can be the case when the magnetic moment of the background is of the same order as the magnetic moment of the sample, and the sample and the background signal from the sample holder are displaced with respect to one another along the axis of the magnet. We will address the issue of non-dipole samples and non-constant dipoles as separate topics.

Because the standard data analysis routines can produce erroneous results we will denote the magnetic moment computed using the constant-dipole model by the designation m^*, while the true magnetic moment of the sample will be denoted by m. For several reasons, the measurements we describe herein were all performed on a Quantum Design Magnetic Properties Measurement System (MPMS). First, each of the authors had an MPMS available in his laboratory. Second, there are an enormous number of these systems currently in use, and the large majority of them are being used to measure superconductors. Third, the MPMS is very versatile, offering a great deal of control over the variables we felt were most important. Of particular importance to us was the fact that the MPMS provides access to the true raw data from the measurement — the digitized values of SQUID voltage as a function of position — that are stored in the data file when using the *All Scans* data-file selection. This makes the raw data available in an easily accessible format, allowing experienced users to analyze the raw data using their own analytical methods and algorithms.

Most of the results of this study should be generally applicable to any magnetometer system in which the sample is moved (or the fields are changed) during the measurement. The specific effects will differ depending on the detection method, detection geometry, output-signal analysis method, the specific magnet used, and the distance the sample is moved. All of these parameters will vary from one instrument to another, so the work reported here strongly suggests the need for similar studies on other specific models of magnetometers. This is particularly true of any magnetometer system which uses an analytical model and data processing algorithms to compute and report some sample parameter, as is the case with virtually all commercial magnetometer systems.

Our goal in performing this work has been to help the users of many different magnetometers understand more fully some of the anomalous behaviors that have been reported over the last several years. Our hope is that this report will stimulate further investigations, research, and analytical modeling into the specific effects that combine to produce the observed measurement results. When reading this report, we hope the reader will take enough time to study all of the figures carefully. The specific choice of figures was made for the purpose of systematically building the concepts necessary to understand the important issues, but in many of the graphs, different properties are plotted as a function of the position, z, along the axis of the magnet, making it possible to confuse the various plots under a cursory examination.

B. Experimental

This section provides a brief introduction to the methods used in these studies as well as a brief discussion of some of the considerations taken into account. A much more detailed description of the operation of the MPMS and reasons behind various considerations can be found in Appendix B and the manuals provided with the MPMS. In the following we have tried to accommodate users of both *Système Internationale d'Unités*, or SI, and *cgs* systems of units by giving expressions in both forms and using (SI) and (cgs) to indicate the applicable units.

1. The Sample

The sample used in these studies was a $YBa_2Cu_3O_7$ (YBCO) thin film, approximately 3000 Å thick, prepared by pulsed laser deposition onto a heated 0.5 mm thick [100] $LaAlO_3$ substrate. The substrate had dimensions of 5 mm x 5 mm while the YBCO film was patterned into a 2 mm diameter circle. The film had a superconducting transition temperature T_c = 90 K and the superconducting material had a mass of about 5 x 10^{-6} g. The magnetic field was applied perpendicular to the plane of the film (along the c axis). These films generally exhibit large values of the critical current density, J_c, with values $J_c \approx 10^6$ A/cm^2 at T = 77 K being fairly typical.

When measuring a sample with a large magnetization value, e.g. a superconductor, it is often important to consider *demagnetization effects*. For an elliptically-shaped sample, the total H field inside the sample is given by $H = H_0 - H_d$, where H_0 is the applied field produced by the current in the magnet coil and H_d is the demagnetization field. The demagnetization field is given by $H_d = -NM$, where N is a shape-dependent demagnetization factor and M is the magnetization of the material. For a long thin sample in a parallel field $N \approx 0$, while for a short flat sample in a perpendicular field the demagnetization correction (NM) can be enormous. In the case of a superconductor M is negative so that H_d will be positive, which means that the "demagnetization" field actually increases H inside a superconducting sample. The value of N has a range $0 \le N \le 1$ in SI units and $0 \le N \le 4\pi$ in cgs units. It is possible to estimate the demagnetization correction from the initial (virgin) portion of the

magnetization curve, plotting magnetization as a function of applied field, M(H), for samples cooled below T_c in zero applied field, since a slope of M/H = -1 (SI) = $-1/4\pi$ (cgs) is expected for the case in which N = 0.

2. The Measurements

A measurement is performed in the MPMS by moving a sample through the superconducting detection coils, which, as shown in Figure B1, are located at the center of the magnet. The sample moves along the symmetry axis of the detection coil and magnet. As the sample moves through the coils the magnetic dipole moment of the sample induces an electric current in the detection coils. The SQUID functions as a highly linear current-to-voltage convertor, so that variations in the current in the detection coil circuit produce corresponding variations in the SQUID output voltage. Under ideal conditions, the magnetic moment of the sample does not change during transport through the detection coil.

Figure B2(a) shows the position of the various loops making up the second-order-gradiometer detection coil. The position z = 0 cm corresponds to the center of the coil and this is positioned at the midpoint along the length of the magnet. Figure B2(c) shows the output voltage of the SQUID electronics as a function of position V(z) as a sample with a positive, constant magnetic point dipole moment is moved through the pickup coil. This V(z) data can be collected on the MPMS by using the *All Scans* data collection option. As both an example of an *m(z)* plot, as well as to emphasize the position independence of the magnetic moment under ideal conditions, Figure B2(b) shows the *m(z)* = constant plot that corresponds to the V(z) curve in Figure B2(c). Figure B2(e) shows the output signal V(z) for a sample with a constant, negative dipole moment as shown in Figure B2(d).

The signal analysis programs currently provided with the MPMS are designed to analyze a specific type of response: a magnetic dipole of **constant magnitude** moving through this particular type of detection coil (second-order

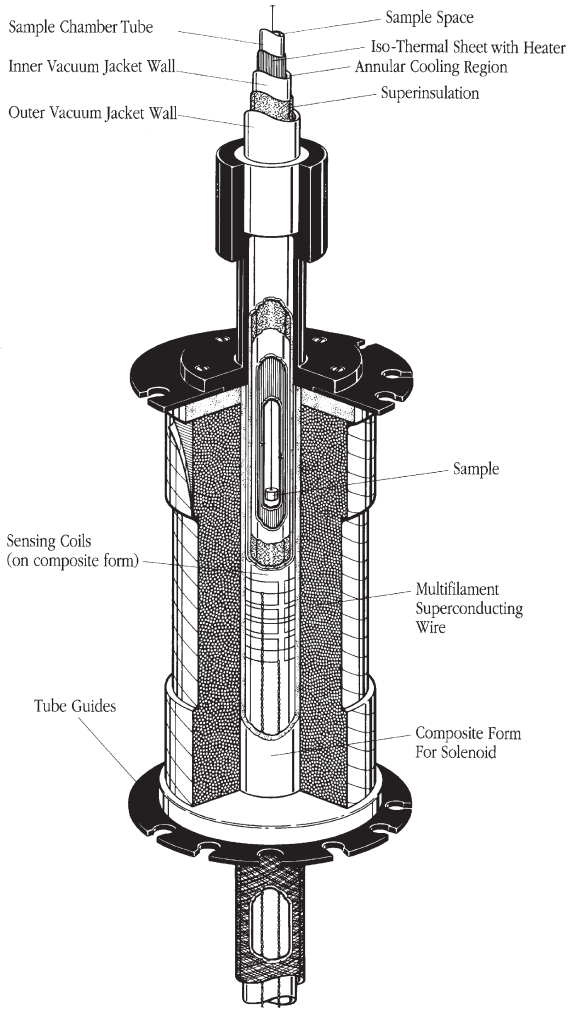

Figure B1(a). The geometrical configuration of the magnet, detection coils and sample chamber.

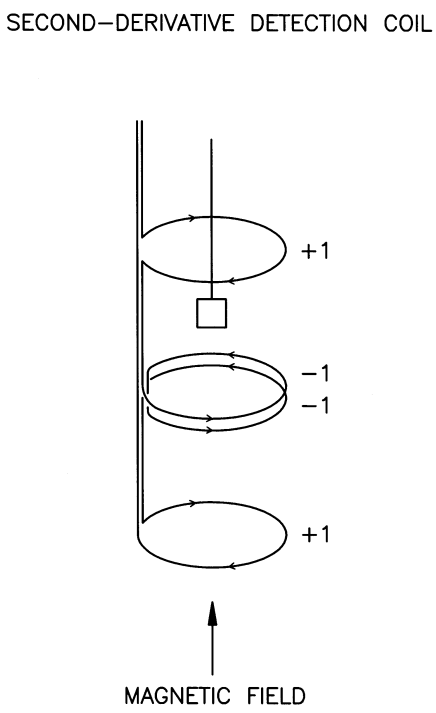

Figure B1(b). The configuration of the second-order gradiometer superconducting detection coil. The coil sits outside of the sample space within the liquid helium bath.

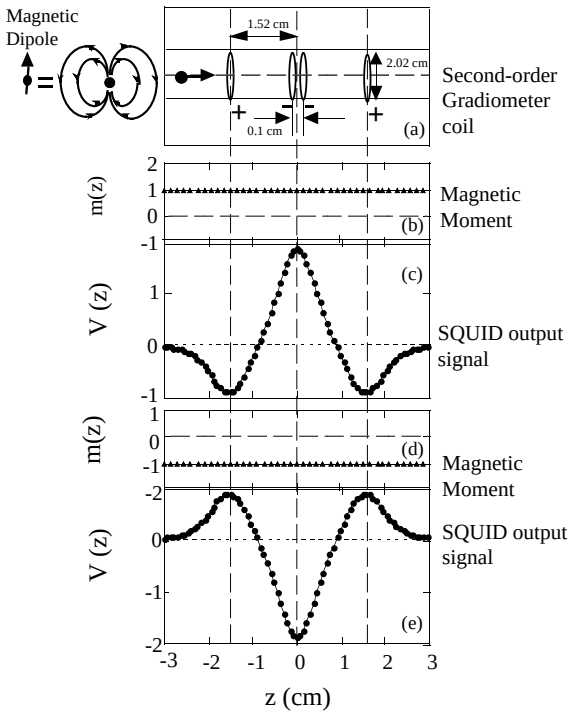

Figure B2. (a) The position z of the loops of the second-order gradiometer detection coil. The position z = 0 corresponds to the center of the coil and this is positioned at the midpoint along the length of the magnet. (b) The ideal behavior of a sample (with a positive value of the magnetic dipole moment) as a function of position, m(z), as it is moved through the detection coil. (c) The output voltage of the SQUID electronics as a function of position V(z) as a magnetic point dipole with the value m(z) = constant > 0, as in (b), is moved through the second-order gradiometer pickup coil. Under ideal circumstances the sample approximates a point dipole and the value of the magnetic moment does not change during the measurement. (d) The m(z) curve for an ideal sample with a negative value of the magnetic dipole moment. (e) The output signal V(z) for a sample with a constant, negative dipole moment shown in (d).

gradiometer). The MPMS provides three methods for analyzing the SQUID output signals. (For further details please refer to Appendix B.) When these signal analysis routines are used for cases in which the output signal deviates significantly from a point-dipole response or if the magnitude of the magnetic moment varies during the measurement (i.e., significant deviations from the *constant-dipole model*), the analysis is not reliable and the magnetic moment value reported by the computer program will not be a true measure of the moment. All of the data analysis routines provided with the MPMS report the magnetic moment of the sample in cgs or electromagnetic units (emu). In many of the cases presented here, the computer fits are often not valid measurements of the magnetic moment, but simply the result of the best computer fit to a measured curve. We will therefore refer to the values produced by computer fits to V(*z*) signals as the *apparent magnetic moment* (designated *m**). When referring to the true (or actual) magnetic moment of the sample, the designation *m* will be used, and even though *m** values are not true magnetic moment values, the emu unit will be used in both cases. In this report the linear regression method is used to produce the *m** values, unless otherwise specified.

Even when the output signal deviates significantly from that of a point dipole or changes during a measurement, the raw data still contain important and fundamental quantitative information about the magnetic properties of the sample. The measured response in these cases is not an error or an artifact, but a full-fledged magnetic measurement of the sample, but for various reasons, the measured response may not correspond to a point dipole-type signal that is easily analyzed to determine the true magnetic moment. Reasons for deviations can include (but are by no means limited to) large background signals, magnetic field non-uniformities and shielding effects of the superconducting magnet. As will be shown, these deviations from a non-ideal dipole response often do not interfere, but rather may even enhance, one's ability to determine properties like the superconducting transition temperature and the vortex-solid phase transition temperature. It will also be shown that in those cases when a quantitative determination of the magnetic moment is actually necessary, one can use an appropriate method for background subtraction when applicable or an appropriate model for the non-dipole response signal.

A common method for identifying the onset of magnetic irreversibility is to make measurements along two paths that expose the sample to very different temperature and/ or magnetic field histories. For superconductors, the most popular method has been the zero-field-cooled/ field-cooled (ZFC/FC) measurement. In this case the sample is first cooled in zero applied field (H = 0) to the lowest measuring temperature. After the temperature has stabilized, a field is applied and data are collected as the sample is warmed to above T_c (the ZFC part). A second set of data is collected as the sample is slowly cooled through T_c in the same field (designated FCC for field-cooled-cooling). In contrast to this, for a field cooled warming (FCW) measurement the sample is cooled to the lowest measuring temperature in the applied field and then measured on warming.

For the FCC measurements presented here, the temperature was decreased in steps of 0.25 K to be sure that no undershooting of the temperature occurred. Because temperature overshooting while warming is less of a problem in general, steps of various sizes were used for

the ZFC measurements. A scan length of 2.5 cm (±1.25 cm) was used in all ZFC and FCC measurements and the sample went through two cycles at each measuring point.

3. Mapping the Magnetic Field Profile

Quantitative information on the small variations in magnetic field over the measuring region are very important to understanding the effects we will be discussing here. Detailed measurements of the magnetic field as a function of position *z* were made under a variety of conditions using a Hall-effect device mounted on a long probe oriented to measure the field component along the axis of the magnet. Measurements were made with the sample space at a temperature of 300 K. The probe was attached to the MPMS sample transport to take advantage of its precise positioning capabilities. Measurements of the magnetic field profile were usually made over a 6 cm scan length ($z = \pm 3$ cm). Using the Hall-effect device, the magnetic field could be measured to a precision of 0.01 Oe in low fields, and about 1 part in 10^5 at higher fields.

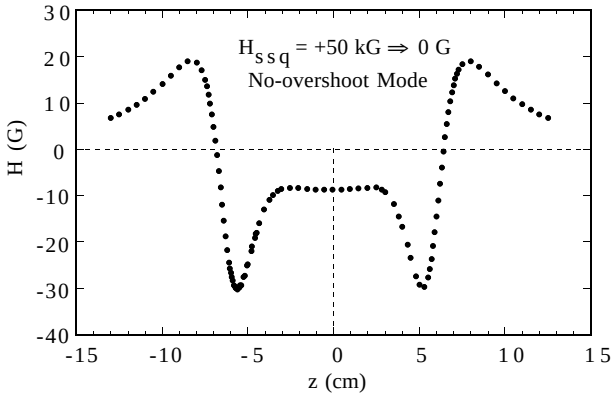

Figure B3. Even when the transport current in the superconducting magnet has been reduced to zero, the trapping of flux in the superconducting windings can result in a distribution of non-zero fields in the magnet. The axial component of the magnetic field is shown as a function of position from z = -13 to +13 cm, where the midpoint along the magnet's length is defined as z = 0.

Figure B3 shows a magnetic field profile H(*z*) for the magnet after the field has been changed from a setting of +50 kOe to a setting of zero. This particular H(*z*) profile shows the magnetic field variations from $z = -13$ to +13 cm. Even though the transport current flowing through the magnet is zero, due to flux trapping in the superconducting wire from which the magnet is constructed, the magnetic field is not zero except at a few points. For the *m** measurements presented in this report, the sample was scanned over 2.5 cm in the most uniform region at the center of the magnet.

4. Altering the Magnetic Field Uniformity

The MPMS system provides four different methods for changing the magnetic field in the system. The *no-overshoot*, *oscillate*, and *hysteresis* modes are useful for routine changes between arbitrary starting and ending values, while the *magnet reset option* provides a special method for eliminating nearly all of the trapped flux from the superconducting MPMS magnet by driving the magnet normal (non-superconducting). More detailed descriptions of the operation and attributes of each method are presented in Appendix B.

The specific magnet field profile H(*z*) depends on several factors including the field-change method used and the previous history of magnetic field settings. The field uniformity increases in the order of: no-overshoot, oscillate, magnet reset. The actual field profile is fairly reproducible for the oscillate and reset modes. In contrast to this, the no-overshoot mode can produce field variations with a large range of values, however, the trends we show here, particularly those associated with different sequences of field changes, are fairly reproducible.

5. Definitions of Fields, Field Sequences, and Units

For the purposes of the discussions here, the unit gauss (or G) will be used when referring to either the magnetic field (usually denoted H) or the magnetic flux density (usually denoted B). The relationship between B and H is given by $B = H + 4\pi M$ (cgs), where M is the magnetization of the sample and H is the field produced by the magnet. The cgs unit for H is oersted (or Oe) while the cgs unit for B is the gauss, however as a unit of measure 1 Oe = 1 G, so in practice gauss is often used for H. The SI unit for H is A/m, while tesla or Wb/m^2 is used for B, with B = 1 tesla = 10,000 G and $B = \mu_0 H + \mu_0 M$. In addition to units, several different field designations will be used here. H will refer to the actual field (which can be experimentally measured) produced by the magnet, while H_{set} will refer to the field that is determined — using the appropriate calibration coefficient — from a measurement of the current flowing from the power supply through the magnet. The difference between the actual field H and H_{set} is not due to errors in the calibration, but rather to flux trapping and the hysteretic nature of superconducting magnets.

In addition to the different field designations used here, there will be frequent references to the particular sequence of magnetic field settings. As will be shown, the particular sequence of field changes has a significant effect on the magnitude and spatial dependence of the magnetic field uniformity. In all the cases described, the field will be set to zero ($H_{set} = 0$) from either $H_{set} = +50$ kG or $H_{set} = -50$ kG, in which case these sequences of field changes will

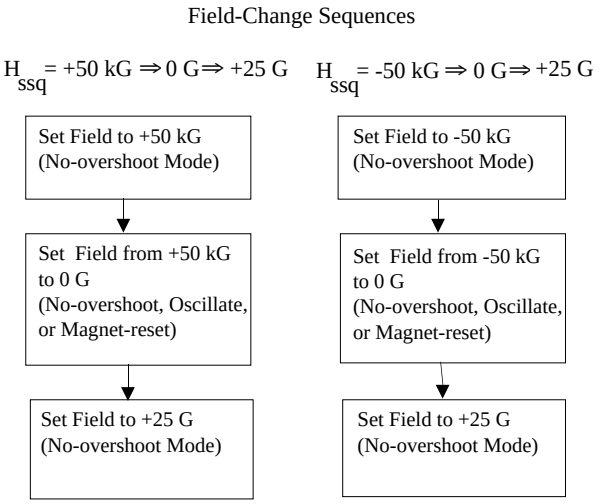

Figure B4. Because there will be frequent references to the particular order of magnetic field settings used prior to starting a given measurement, a convention for writing these field changes is defined here. H_{ssq} refers to the sequence of H_{set} values to which the magnet was set in order to obtain the particular magnet state used in the measurement. As will be shown, the sequence of field changes effects the spatial dependence of the magnetic field uniformity.

be noted by H_{ssq} = +50 kG ⇒ 0 G or H_{ssq} = -50 kG ⇒ 0 G, respectively. In some cases an additional field, i.e. the measuring field, will then be set from one of these two H_{set} = 0 conditions (or remanent states). In the particular case that the final field setting is H_{set} = +25 G, the two sequences would be noted as H_{ssq} = +50 kG ⇒ 0 G ⇒ +25 G and H_{ssq} = -50 kG ⇒ 0 G ⇒ +25 G. These definitions are described schematically in Figure B4. In some of the studies to be described, either H_{ssq} = +50 kG ⇒ 0 G or H_{ssq} = -50 kG ⇒ 0 G will be used above the superconducting transition temperature T_c, and then the measuring field will be set at a temperature below T_c.

C. Field Uniformity and Properties of Superconducting Magnets

When a magnet is used to produce magnetic fields over a wide range of values, there is a practical limit on the spatial uniformity of the field that can be produced. Uniformity can be improved by incorporating a larger magnet like those used in high-resolution NMR, in which case the uniformity is usually optimized at the single field value at which the magnet will be operated. When measurements are to be made over a wide range of fields, the larger magnet will slow operation, increase the physical size of the system, and, in the case of superconducting magnets, increase the liquid-helium boil-off. The region midway between the ends of a solenoidal magnet is generally the region with the smallest field curvature and greatest uniformity. The superconducting magnet used in the MPMS has additional windings toward the ends of the magnet to further reduce the curvature of the field near its central region. The detection coils are centered along the length of the magnet to take advantage of the field uniformity near the center. Variations in field due to sample motion during a measurement can be further reduced by shortening the scan length so the measurement is made in only the most uniform portion of the magnet.

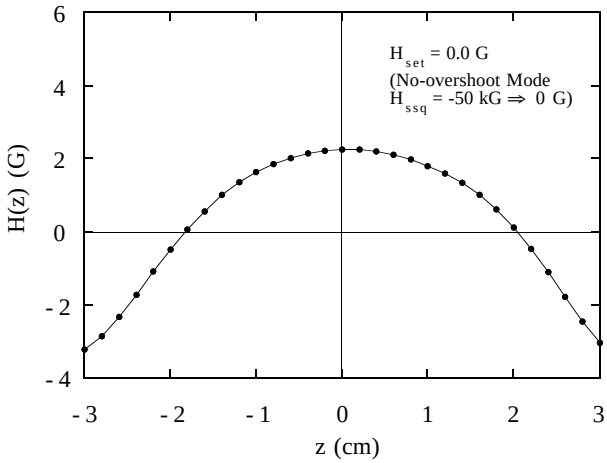

Figure C1. The magnetic field as a function of position z along the axis of a 55-kG solenoidal magnet, H(z), in an MPMS magnetometer after reducing the transport current through the magnet to zero (remanent profile H_{set} = 0) from a field of H_{set} = +50 kG using the no-overshoot mode. This H(z) profile was measured directly using a Hall-effect device mounted on a probe. Note that the point midway along the length of the magnet (center) is defined as z = 0.

Figure C1 shows the magnetic field as a function of position, *z*, along the axis of a 55-kG solenoidal magnet in an MPMS magnetometer after reducing the transport current of the magnet to zero (H_{set} = 0) from the field setting H_{set} = -50 kG (H_{ssq} = -50 kG ⇒ 0 G) using the no-overshoot mode. This H(*z*) profile was measured directly using a Hall-effect device mounted on a probe. As shown in Figure C1, from *z* = -3 to +3 cm the field changes by about 5 G and is fairly symmetric about the center. Using a computer fit, the shape of the H(*z*) curve in Figure C1 can be approximated by the relation $H(z) = -2.99 - 0.11\,z + 0.65\,z^2$ G. (Additional information about field uniformity at longer distances from the center of the magnet can be found in Quantum Design's Technical Advisories #1 and #6.)

Figure C2 shows a comparison between the H_{set} = 0 profiles obtained using the no-overshoot mode for two different field-change sequences. In one case, the field

was set to zero (H_{set} = 0) starting from a field setting of H_{set} = +50 kG (H_{ssq} = +50 kG ⇒ 0 G) and, in the other case, the field was set to zero starting from a field with the opposite polarity, H_{set} = -50 kG (H_{ssq} = -50 kG ⇒ 0 G). These two *remanent* profiles are nearly symmetric (a mirror reflection) about H = 0. The differences in the final state of the magnet (the specific spatial dependence of the field) and how the state depends on the particular sequence of magnetic field changes is crucial to understanding the various anomalies that can occur when measuring superconducting samples. The different H(*z*) profiles produced by the two different sequences will result in very different magnetic-field histories when a sample is measured under these two different conditions. (Magnetic-field history refers to the sequence of magnetic fields to which the sample itself is exposed. This includes the field changes due to changing the current in the magnet, but it also includes the field changes that occur when the sample is moved to different positions in the magnet where the field value is different due to the field non-uniformities.) For samples exhibiting irreversible (hysteretic) properties (e.g., superconductors and ferromagnets), the value of the magnetization can be a very strong function of the magnet-field history.

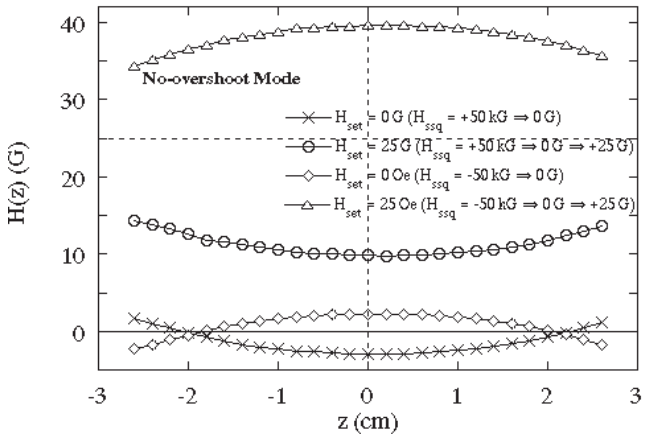

Figure C2. A comparison between the remanent profiles obtained using the no-overshoot mode. In one case, the field was set to zero (H_{set} = 0) from a field setting H_{set} = +50 kG and, in the other case, the field was set to zero from H_{set} = -50 kG. Also shown is the effect of setting H_{set} = +25 G using the no-overshoot mode from each of the two remanent states.

Figure C2 also shows the effect of using the no-overshoot mode to set an H_{set} = +25 G field from each of these remanent states (H_{ssq} = +50 kG ⇒ 0 G ⇒ +25 G and H_{ssq} = -50 kG ⇒ 0 G ⇒ +25 G). The profiles essentially retain the same shape and relative amplitude variation, however neither profile is displaced by +25 G from its H_{set} = 0 position. Instead, the H_{set} = +25 G profiles are now nearly symmetric about H = +25 G, with the profile associated with an initial setting of H_{set} = -50 kG displaced by an additional +9 G and the profile associated with the initial setting of H_{set} = +50 kG displaced by about -9 G.

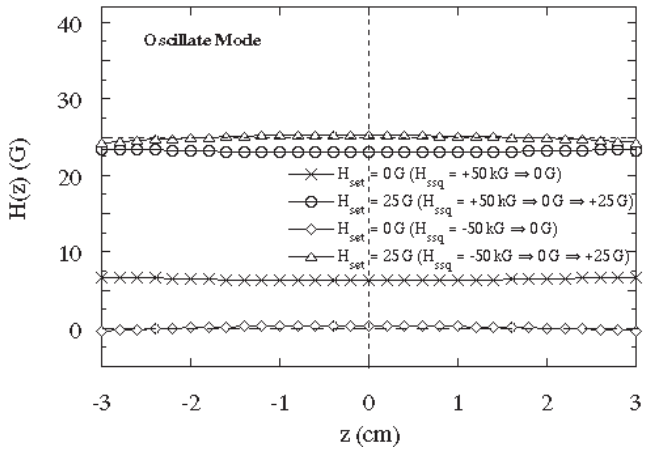

Figure C3. A comparison between the remanent profiles obtained using the oscillate mode. In one case, the field was set to zero (H_{set} = 0) from a field setting H_{set} = +50 kG and, in the other case, the field was set to zero from H_{set} = -50 kG. Also shown is the effect of setting H_{set} = +25 G from each of the H_{set} = 0 states using the no-overshoot mode.

Each of the field-change methods available (*no-overshoot*, *oscillate*, and *magnet reset*) on the MPMS will produce a different H(*z*) profile. Figure C3 shows the remanent profiles produced when the oscillate mode is used for the same field-change sequences that were used to produce the curves in Figure C2. By comparing the amplitudes of the curves in Figure C2 and C3, it is clear that using the oscillate mode reduces the amplitude of the non-uniformity considerably compared to the no-overshoot mode, with H(*z*) varying by only 0.4 G from *z* = -3 to 3 cm for the oscillate mode compared with an H variation of about 5 G over the same length when using the no-overshoot mode. The shape of the H_{ssq} = +50 kG ⇒ 0 G curve in Figure C3 can be approximated by $H(z) = 6.23 - 0.0024\,z + 0.056\,z^2$ G. Note that when using the oscillate mode, the H_{set} = 0 curves are not symmetric about H = 0. Instead the H_{ssq} = -50 kG ⇒ 0 G curve straddles H = 0 while the H_{ssq} = +50 kG ⇒ 0 G curve is displaced by about +6 G from H = 0. Remarkably, when the magnet is now set to H_{set} = +25 G (using the no-overshoot mode only for this last field change), both H(*z*) profiles fall fairly close to H = +25 G. However, the shapes of the profiles change somewhat from the shape observed at H_{set} = 0, which is particularly true for the H_{ssq} = -50 kG ⇒ 0 G curve.

The other method that can be used to alter the H(*z*) profile is the magnet reset option. The remanent profiles produced for the cases when the field is set to H_{set} = 0 from H_{set} = +50 kG and -50 kG using the magnet reset, are shown

in Figure C4. The amplitudes of the curves in Figure C4 are very small, with an H(*z*) variation less than 0.1 G from *z* = -3 to +3 cm, which compares with an H(*z*)-variation of about 5 G when using the no-overshoot mode and 0.4 G using the oscillate mode. The H(*z*) curve can be approximated by $H(z) = -0.501 + 0.020\ z + 0.0023\ z^2$ G. The H_{set} = 0 curves are not symmetric about H = 0. In this case the H_{ssq} = +50 kG ⇒ 0 G curve straddles H = 0 while the H_{ssq} = -50 kG ⇒ 0 G curve is displaced by about -0.6 G from H = 0. The Earth's magnetic field is about 0.5 G and the system was not magnetically shielded in these studies. When the magnet is now set to H_{set} = +25 G (using the no-overshoot mode for only this last field change), both H(*z*) profiles are now fairly close to H = +23 G and the shapes of the profiles change somewhat from the shape observed at H_{set} = 0. In both cases the H(*z*)-variation from *z* = -3 to +3 cm is still smaller than in either the no-overshoot or oscillate modes, varying by less than about 0.1 G.

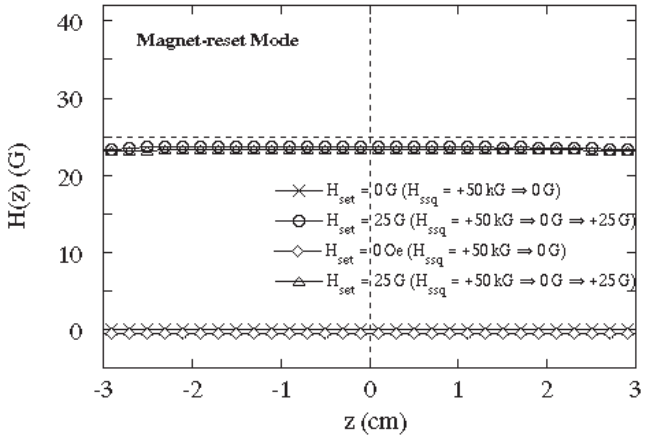

Figure C4. A comparison between the remanent profiles obtained using the magnet-reset option. In one case, the field was quenched to zero (H_{set} = 0) from a field setting H_{set} = +50 kG and, in the other case, the field was quenched to zero from H_{set} = -50 kG. Also shown is the effect of setting H_{set} = +25 G using the no-overshoot mode from each of the remanent states.

We want to emphasize that the field profiling [H(*z*)] measurements and the experimental data presented in this report were collected from a single MPMS instrument. In particular, it is not generally true that different magnets on different instruments will all behave in the same way, even if the magnet is the same model as the one used to collect the data described in this report. Experimental measurements at Quantum Design have shown that the remanent fields in the MPMS magnets vary significantly from one instrument to another. We have no explanation for this behavior, but we speculate that the detailed nature of the remanent fields in any particular magnet probably depends strongly on the microscopic structure of its superconducting wire, which can ultimately be traced back to the metallurgical properties of the original materials and the exact process by which the wire is fabricated. In any event, we want to warn the reader that one cannot directly apply the quantitative results on field profiles presented in this report to any other magnetometer system. While the general trends observed for field change sequences should apply to all MPMS systems, it is important to properly characterize the field profiles experimentally for your own individual system.

D. Effects of Field Uniformity on Superconductor Measurements

1. Magnetic Properties of Superconductors - Briefly

The magnetic behavior of superconductors is fairly complicated. The complicated nature of their behavior is due in part to the fact that the magnetic behavior of a superconductor can depend very strongly on the form of the material (e.g., polycrystalline or single crystal) as well as on the density and types of defects present in the specific sample. This also means that the magnetic behavior can be altered by processes that effect the material's structure.

When a small magnetic field is applied to a superconductor, supercurrents induced near the surface of the superconductor can completely screen the applied magnetic field from the interior of the sample (B = 0 inside). This corresponds to the initial portion of the magnetization as a function of applied field, M(H), curve in Figure D1, which has a slope of -1 (SI) [$-1/4\pi$ (cgs units)]. This regime is often referred to as the Meissner state. For an ideal type-II superconductor the sample's interior would remain completely screened up to the lower critical field H_{c1} after which the magnetic field penetrates into the sample in the form of quantized lines of magnetic field (flux vortices). The amount of flux that has penetrated into the sample is proportional to the flux density, B. The relationship between B, H, and M is also shown in Figure D1. A key point about the ideal M(H) curve shown in Figure D1 is that it is reversible, with M following the same curve both on increasing and decreasing H. A superconductor exhibiting this ideal behavior would not be able to support a supercurrent for magnetic field levels above H_{c1}, because under these conditions the penetrating magnetic flux lines provide a mechanism for the dissipation of the supercurrents.

In order to support a supercurrent above H_{c1}, the flux vortices in a superconductor must be immobilized. When a transport current flows in an ideal superconductor with penetrating flux lines, the Lorentz force ($\mathbf{F}_L = \mathbf{J} \times \mathbf{B}$) acts on the vortices which results in motion of the vortices through the sample. The moving vortices result in

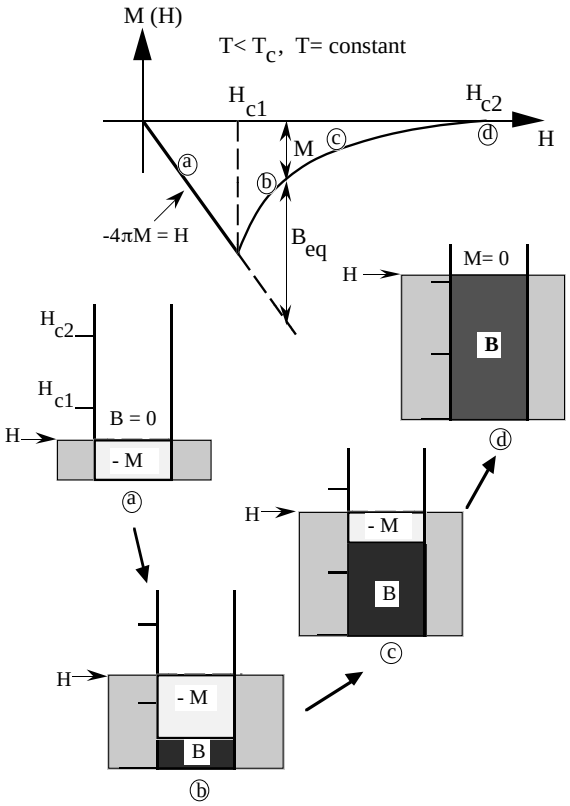

Figure D1. The ideal M(H) curve for a reversible type-II superconductor. Below the lower critical field, H_{c1}, the superconductor completely screens out the applied magnetic field H (or H_a). Since B = H + 4πM (cgs), then M = -H/4π for H < H_{c1}. Just above H_{c1} some of the applied magnetic field penetrates into the superconductor in the form of flux vortices. The amount of flux penetration is proportional to B and, as the applied field continues to increase, a larger fraction of the applied field penetrates into the superconductor. At the upper critical field H_{c2}, the applied field fully penetrates (B ≈ H) and the sample goes normal.

dissipation giving the superconductor a resistance. An effective mechanism for immobilizing flux vortices is to introduce defects into the material which can serve as sites for "pinning" the flux vortices. This pinning is usually the result of a flux vortex having a lower energy at a defect. With a sufficiently large density of defects present in the superconductor, a supercurrent can be supported up to the critical current J_c, which is where the Lorentz force associated with the applied current just exceeds the pinning force. Flux motion is only one of the mechanisms that can limit J_c. Clearly the dissipation mechanism that results in the smallest J_c (the one that produces dissipation at the smallest value of J) is the one that will determine J_c for the sample.

One important consequence of flux pinning is that the M(H) curve will now be irreversible below the vortex-solid transition. This means that the M(H) loop will be hysteretic, following a different M(H) curve for increasing H than for decreasing H. The hysteresis will increase as the pinning strength increases and there will be a corresponding increase in J_c. This effect is the basis of the Bean Critical State model which can be used to relate the J_c of a sample (a transport property) to the sample's magnetization using a geometrical factor (see Appendix A for a brief description of the Bean model).[2] It is important to realize, however, that irreversibility results in a history dependence for properties like magnetization, so that the sequence of magnetic field changes and temperature changes can both effect the value of the magnetization measured for an irreversible sample. An accurate (or even relevant) measurement of many properties will require the proper preparation (a particular sequence of field and temperature changes) to place the sample in the state where a meaningful measurement can be made.

2. Effects in the Reversible State

As a sample is moved along the axis of the magnet during a measurement in a magnetometer, the field H at the sample will change as a function of position due to the non-uniformity of the magnetic field. A very important consequence of this changing local field is that this will produce a **position dependence for the true magnetic moment** of the sample, *m*(*z*), since the sample's moment depends on the applied field in which the sample actually resides. Superconductors in the Meissner state have a very large, negative volume susceptibility M/H = χ = -1/4π (cgs units) ~ -0.08 emu/cm^3/G. For a sample of a superconducting material having a density of 5 gram/cm^3 and a mass of 1 milligram, a field change of about 5 G would correspond to a magnetic moment change of about 8 x 10^{-5} emu. For a thin superconducting sample in a perpendicular field, the demagnetization effects would produce much larger magnetic fields leading to correspondingly larger changes of the magnetic moment with position.

For an ideal superconductor in the Meissner state, the superconductor acts like a perfect, reversible diamagnet. Thus, the magnetic moment *m* is proportional to the negative of the applied field. To completely screen out the applied field from the interior of the superconductor, shielding currents near the surface of the superconductor increase in proportion to the applied field. Thus, small positive increases in the magnetic field at the sample will result in the magnetic moment of the Meissner-state superconductor becoming more negative. Figure D2 shows the measured H(*z*) profile for a field setting H_{set} = 0 which was set using the no-overshoot mode from a setting H_{set} = -50 kG. The local H experienced by the sample

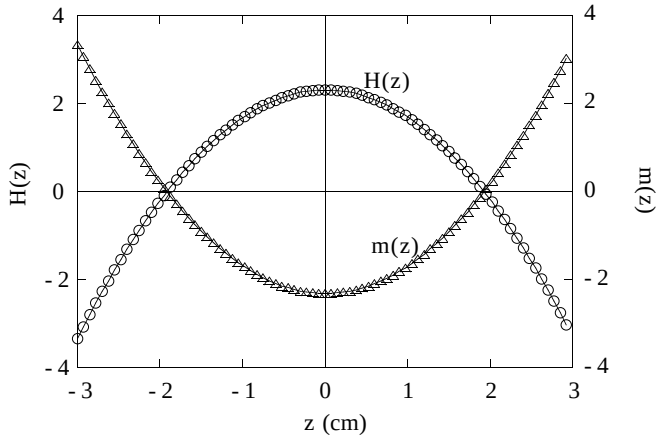

Figure D2. The measured H(z) profile for a field set to H_{set} = 0 using the no-overshoot mode from H_{set} = -50 kG (H_{ssq} = -50 kG ⇒ 0 G). m(z) is a calculation of the magnetic moment of a reversible superconductor as it experiences this particular H(z) dependence. m is not constant during a measurement, but rather varies proportionally with the local H value as the sample moves along z. In this calculation the second-order polynomial fit to the H(z) profile in Figure C1 was used.

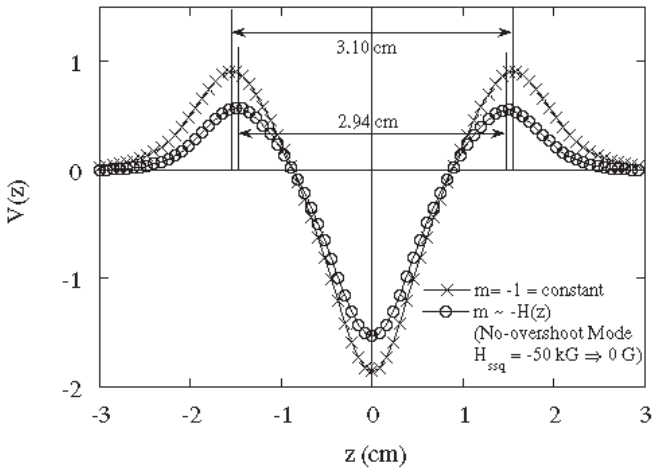

Figure D3. The SQUID output signal V(z) for a dipole moving through the detection coil for the ideal situation in which the magnitude of the moment is unchanged during the measurement, i.e. m(z) = negative constant. Also, the SQUID output signal V(z) for a superconductor sample in the Meissner state having the m(z) dependence shown in Figure C1.

initially increases as the sample moves from its starting position, plateaus near the center of the magnet (z = 0), and then decreases. A calculation of the effect of this particular non-uniform field profile (non-uniformity) on the position dependence of the magnetic moment, $m(z)$, of a reversible superconductor is also shown in Figure D2, where it can be seen that $m(z)$ initially decreases then increases after the sample passes through the center of the magnet. Thus, for a superconductor in the Meissner state, $m(z)$ is not constant during a measurement, but rather will have a component that varies proportionally with the field variations it experiences during the measurement.

As shown in Figure D3, in the case of a superconducting sample, the effects of field non-uniformity on the SQUID output signal can be surprisingly significant. The open circles in Figure D3 have been calculated to show the expected SQUID output signal, V(z), for a superconducting sample with the position-dependent magnetic moment, $m(z)$, shown in Figure D2. The $m(z)$ curve was displaced by an additive constant so that $m(z = -3) = 0$ at the starting point of the scan. (For comparison, the crosses in Figure D3 show the SQUID output signal V(z) for the position-independent constant-dipole model where $m(z)$ = constant, but $m(z)$ is NOT zero.) A crucial observation here is that, since the magnetic field was originally set to zero (H_{set} = 0), there should have been no signal at all from the sample, so in this particular case the entire SQUID output signal is an artifact of the non-uniform field caused by flux trapped in the magnet. Note that this spurious output signal is very similar in shape to the ideal constant-dipole signal, including the symmetry about z = 0, but the extrema are now located closer to z = ±1.47 cm than they are to the z = ±1.55 cm positions associated with the constant-dipole model. It is neither accurate nor useful to consider this artifact signal as a measurement of the sample's magnetic moment. Even though the analysis algorithm will return a value for the magnetic moment when it operates on this artifact signal, this "apparent magnetic moment" value is merely a best fit to the SQUID output signal which is produced by local field changes during the motion of the sample. In fact, for a superconductor in the Meissner state, *m(z)* should be constant and equal zero when H = 0. The measured response is a true magnetic measurement of the sample, however, it is not the particular measurement which the analysis programs were designed to analyze.

V(z) signals for which the extrema occur closer to z = 0 than those of point-dipole signals have been observed for years when measuring superconductors, particularly near T_c.[3,4] The origins of these signals have been very difficult to explain, and models employing contributions from higher-order magnetic multipoles has failed to account for these observations. Recently, however, it was shown that these kinds of signals could be produced when the magnetic moment has a spatial dependence,[5,6] as shown in Figure D3.

It was shown in Section C (see Figure C2) that the H(z) profiles for the H_{ssq} = +50 kG ⇒ 0 G and H_{ssq} = -50 kG ⇒ 0 G sequences were essentially mirror images of one another about H = 0. Since the magnetic moment of the

superconductor is proportional to the field, H, in which it resides, it follows that a pair of H(z) curves that have mirror symmetry about H = 0 will produce a pair of m(z) curves that have mirror symmetry about m = 0. This can be seen by comparing the curves with open circles in Figures D3 and D4, which are clearly mirror images about m = 0. This example is meant to help to reinforce the conclusion that the V(z) output signal in these cases is merely a particular magnetic response resulting from transporting a superconducting sample through a non-uniform magnetic field, rather than a measurement of a dipole moment of constant amplitude. Even though they are essentially artifacts, computer fits to the V(z) curves shown in Figures D3 and D4 would produce moment values of the same magnitude but opposite in sign. Specifically, a negative apparent moment m* would result for the V(z) curve in Figure D3 and a positive m* for the curve in Figure D4.

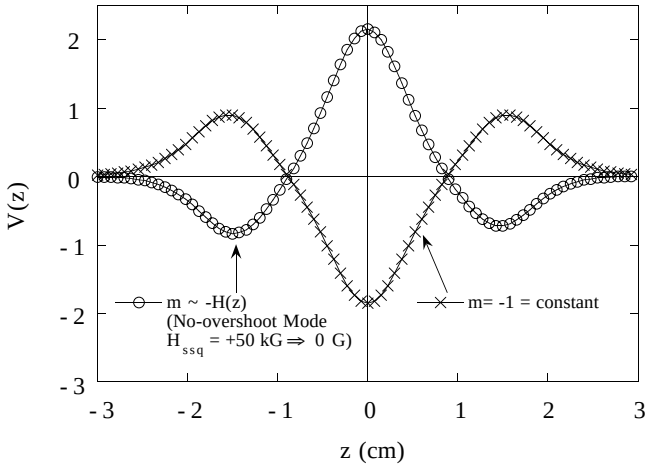

Figure D4. The SQUID output signal, V(z), for a superconductor sample in the Meissner state calculated using the H(z) profile resulting from the field-change sequence H_{ssq} = +50 kG ⇒ 0 G. The SQUID output signal for the ideal case (m = negative constant) is plotted for comparison.

3. Effects in the Irreversible State

The onset of irreversibilities dramatically changes the magnetic properties of a superconductor. Prior to the discovery of high temperature superconductors (HTS) it was usually assumed that the onset of irreversibilities coincided with the upper critical field, H_{c2}, which is the boundary that separates the superconducting and normal (non-superconducting) states of a type-II superconductor. In HTS materials observations of a large separation in field (or temperature) between the onset of irreversibilities, and the apparent onset of the strong diamagnetic response associated with superconductivity, led to the identification of a previously unexpected phase transition, now known as the vortex-solid phase transition. This phase transition separates a higher-temperature phase in which J_c is always zero, and flux vortices cannot be pinned, from a lower-temperature phase in which $J_c > 0$ and vortices can be pinned. Whether or not one should regard the $J_c = 0$ phase as superconducting remains a controversial question (mostly of semantics) because the $J_c = 0$ phase cannot support a supercurrent without dissipation (resistance) yet there appears to be a significant density of Cooper pairs present in this phase. It can be difficult to reconcile that the flux vortices causing the dissipation are entities associated with superconductors and local supercurrents, yet the word "superconductor" suggests a macroscopic zero resistance state.

A common method for identifying the onset of irreversibility is to make measurements along two different paths that expose the sample to very different temperature and/or field histories.[7] As mentioned earlier, for superconductors the most popular method has been the zero-field-cooled/ field-cooled (ZFC/FC) measurement. In this case the sample is first cooled in zero applied field to the lowest measuring temperature (ZFC). After temperature stabilization, a field is applied and data are collected as the sample is warmed to above T_c. Another set of data is then collected as the sample is slowly cooled in the same field from above T_c, which is designated FCC for field-cooled-cooling.

Figure D5(a) shows the ZFC- and FCC-m*(T) curves measured for the YBCO film in which the magnetic field is applied perpendicular to the film, parallel to the crystallographic c-axis. [Figure D5(b) is an expanded view of the data over a narrow temperature range near T_c.] The behavior observed here is not particular to HTS materials. These films are generally regarded as strong pinning and have very high J_c values below the vortex-glass transition. The scan length was 2.5 cm (z = ±1.25 cm) in all cases and the apparent moment values, m* , were determined using the linear regression routine to analyze the SQUID-output V(z) curves. For the ZFC curves the field was set to H_{set} = 0 at a temperature above T_c from either H_{set} = +50 kG or H_{set} = -50 kG using either the no-overshoot, oscillate, or reset modes. The sample was then cooled to the lowest measuring temperature (T = 5 K) where the field was set to H_{set} = +25 G using the no-overshoot mode. FCC curves were measured immediately after the corresponding ZFC curve. Figure D5 shows both sets of ZFC- and FCC-m*(T) curves measured in H_{set} = +25 G for the two different field-change sequences.

From Figure C2 it follows that the two sequences H_{ssq} = +50 kG ⇒ 0 G and H_{ssq} = -50 kG ⇒ 0 G will generate H(z) profiles that are mirror images of one another. Similarly, there is a remarkable mirror symmetry between the two FCC-m*(T) curves of Figure D5, including even

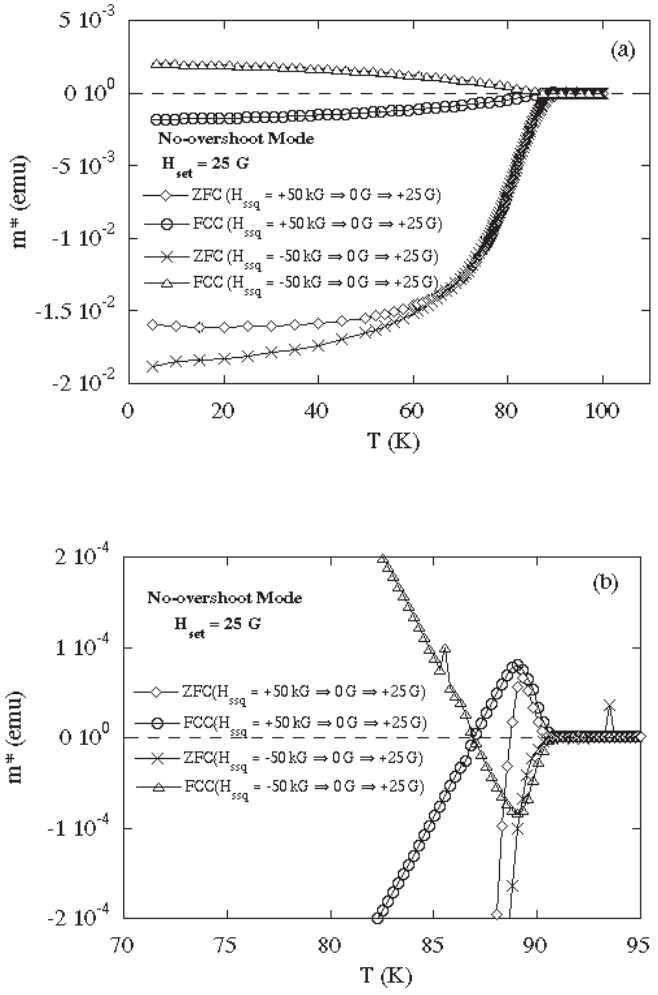

Figure D5. (a) ZFC- and FCC-$m^*(T)$ curves measured at H_{set} = +25 G. H_{set} = 0 was set above T_c using the field-change sequences H_{ssq} = +50 kG ⇒ 0 G and H_{ssq} = -50 kG ⇒ 0 G in the no-overshoot mode, while the measuring field H_{set} = +25 G was applied at T = 5 K in the no-overshoot mode after zero-field cooling. (b) Expanded view of data near T_c.

the reversal near T_c which is clearly seen in Figure D5(b). These curves are nearly perfect reflections of each other across the line $m^* = 0$. This symmetry is also evident in the V(z) plots shown in Figure D6, with the symmetry in both V(z) and $m^*(z)$ observed down to the lowest temperatures. Since the only difference between these two FCC-m^*(T) curves is the field-change sequence used to prepare the field (which has been shown to produce the mirror-image H(z) profiles), we must conclude that the symmetry in the m^*(T) curves arises from the effects of the non-uniform field experienced by the sample as it is transported during measurement. to Figure D5(b), when H_{set} = 0 is set from H_{set} = +50 kG, the FCC-m^*(T) curve initially turns positive as the temperature is lowered below T_c, reaches a maximum and then becomes more negative eventually reaching a plateau at a negative value of m^*.

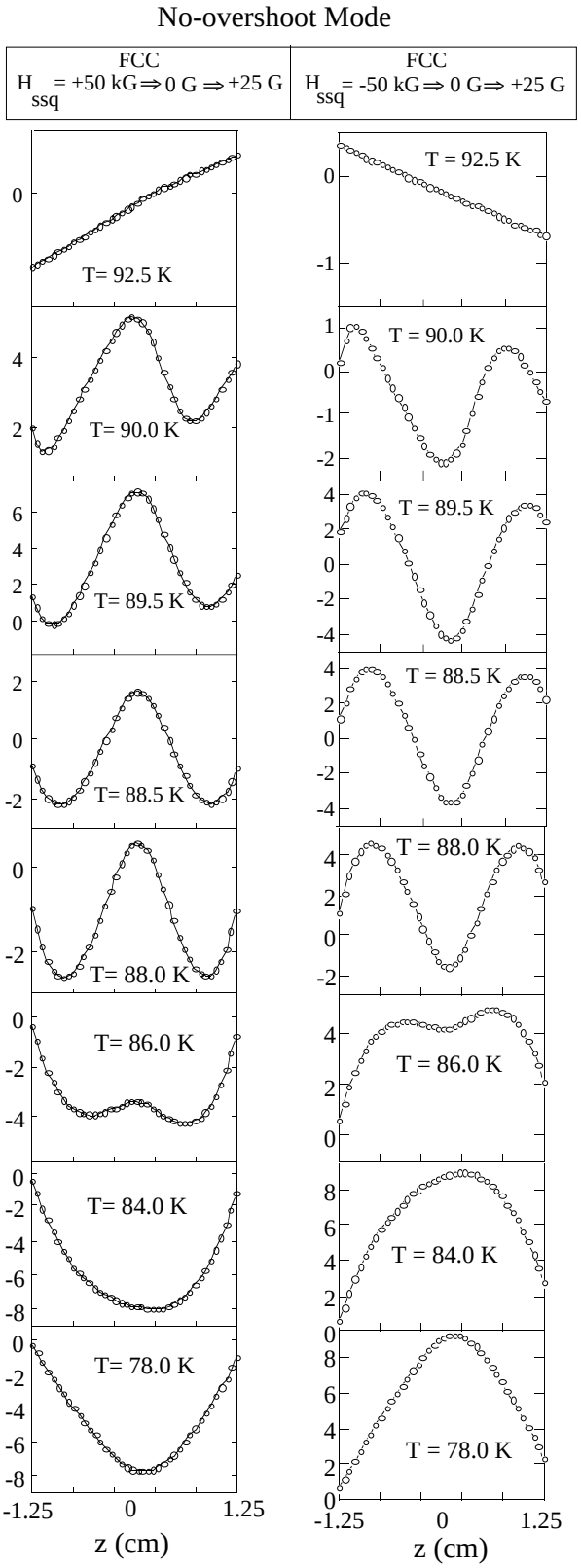

Figure D6(a). The SQUID output signals, V(z), near T_c for the FCC data shown in Figure D5.

The peak in the FCC-m^*(T) curve strongly suggests the presence of two competing effects, both of which are produced by the transport through the field non-uniformities. One of these effects dominates near T_c causing the initial upturn, while the second effect increases with decreasing temperature, eventually dominating the behavior.

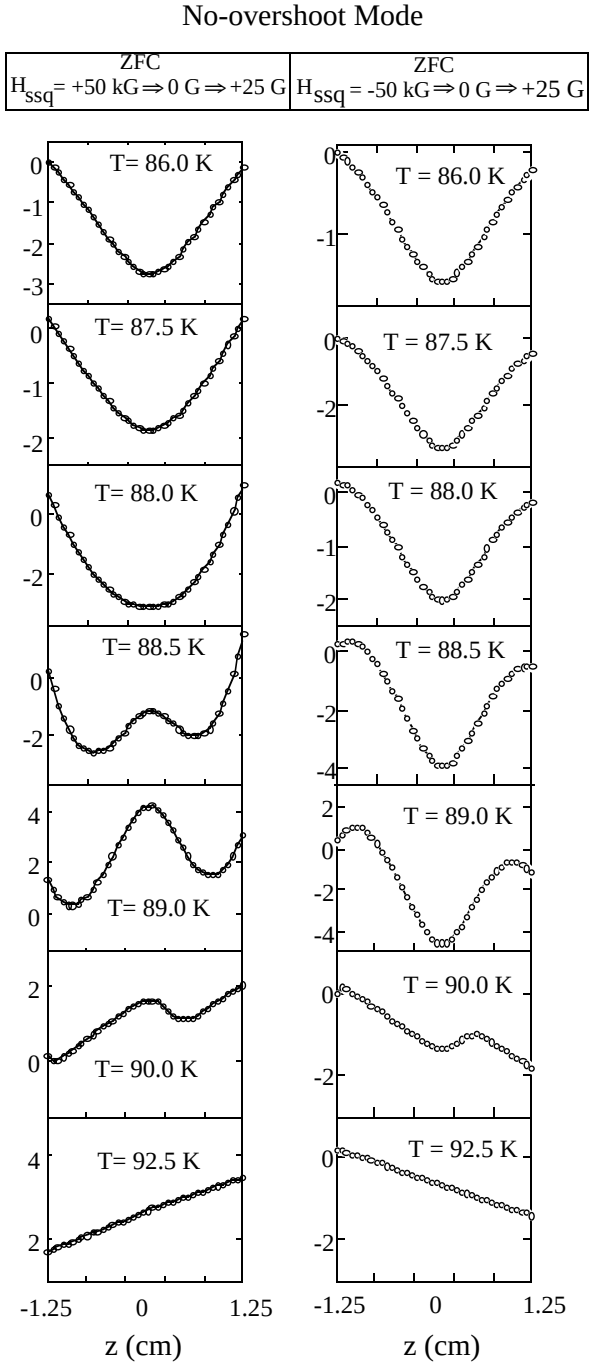

Figures D6(b). The SQUID output signals, V(z), for temperatures below T_c for the ZFC data shown in Figure D5.

Support for two competing effects can be found in the V(z) data of Figure D6(a). At all the temperatures studied the FCC-V(z) curves are related by a simple symmetry operation (rotation about V = constant). At the lowest temperatures the V(z) curves exhibit constant-dipole behavior while at higher temperatures (T > 78 K) it is evident that the extrema that are normally found at z = ±1.25 cm are observed to be much closer to z = 0. The lower-temperature data are consistent with constant-dipole behavior in which the true magnetic moment of the sample does not change much during the measurement process, while the higher-temperature "compressed-peak" behavior near T_c is more consistent with a moment that is changing significantly during the measurement.

At lower temperatures the two ZFC-m^*(T) curves shown in Figure D5(a) are separated by an amount similar to the separation of the two FCC-m^*(T) curves and then for temperatures very close to T_c they become mirror images about m^* = 0. Very close to T_c the ZFC curves follow their corresponding FCC curves breaking away near the peaks in the FCC curves. Figure D6(b) shows the SQUID response V(z) curves for the data collected under ZFC conditions. At the lowest temperatures it can be seen that the V(z) curves are very similar to the ideal SQUID response signal, which is consistent with production of a well-established critical state at the lowest temperature. Near T_c, however, the ZFC-V(z) signals become quite anomalous. For the V(z) data collected using H_{ssq} = +50 kG ⇒ 0 G, it can be seen that the maxima located beyond z = ±1.25 cm in the ZFC-V(z) curves move closer to z = ±1.1 cm as the temperature increases from T = 86 K to 88.5 K. In contrast to this, when H_{set} = 0 is set using H_{ssq} = -50 kG ⇒ 0 G, a new maximum starts to push in near the center (z = 0) of the V(z) curve as the temperature moves above T = 87 K and this new maximum becomes quite clear by T = 88.5 K. Hence, the ZFC-V(z) curves measured using the two different field-change sequences are quite different in the temperature range from about T = 86 K to 89 K. At T = 89 K and above, the curves associated with the different field-change sequences become related by a simple symmetry operation, i.e., reflection of the V(z) data across a line V = constant. This symmetry continues to be observed in the V(z) curves to temperatures above T_c. An examination of the two ZFC-m^*(T) curves, at temperatures of 89 K and above, shows them to be symmetric about m^* = 0.

Since we know that the two field-change sequences produce H(z) profiles that are mirror images of one another, the ability to relate the associated V(z) responses by a simple symmetry operation is fairly strong evidence that the magnetic response observed in the two ZFC-m^*(T) curves near T_c is dominated by the effects of the non-uniform field experienced by the sample as it is transported

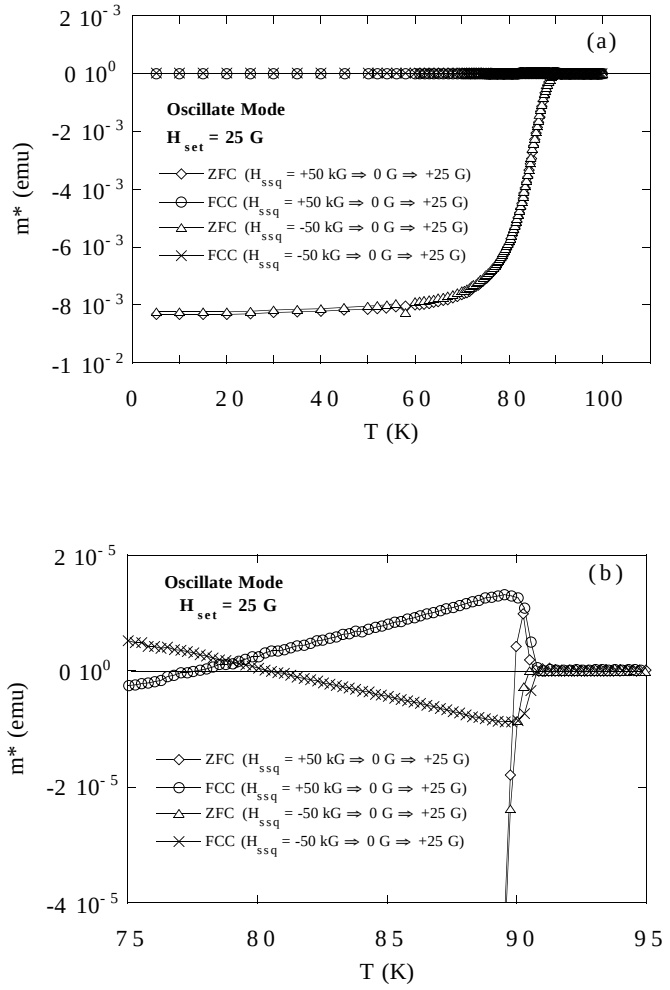

Figure D7. (a) ZFC- and FCC-m(T) curves measured at H_{set} = +25 G. H_{set} = 0 was set above T_c using the field-change sequences H_{ssq} = +50 kG ⇒ 0 G and H_{ssq} = -50 kG ⇒ 0 G in the oscillate mode, while the measuring field H_{set} = +25 G was applied at T = 5 K in the no-overshoot mode after zero-field cooling. (b) Expanded view of data near T_c.*

during measurement. The differences in the two ZFC-*m**(T) curves (around 86 K to 89 K) probably result from the competition of two properties of the superconductor, one property being the pinning of flux, with its associated flux gradients, that is generated by the application of a field only after cooling to low temperature, while the second property is associated with effects arising from transport through the non-uniform field. Near T_c the component of the magnetic moment associated with the trapped flux finally has a magnitude similar to that of the apparent moment associated with the effects produced by the field non-uniformities. Thus, the *m** values observed near T_c are not the actual magnetic moment *m* values of the sample, but rather the best computer fit of the ideal SQUID response to the observed V(*z*) output. However, at lower temperatures the results should be an accurate

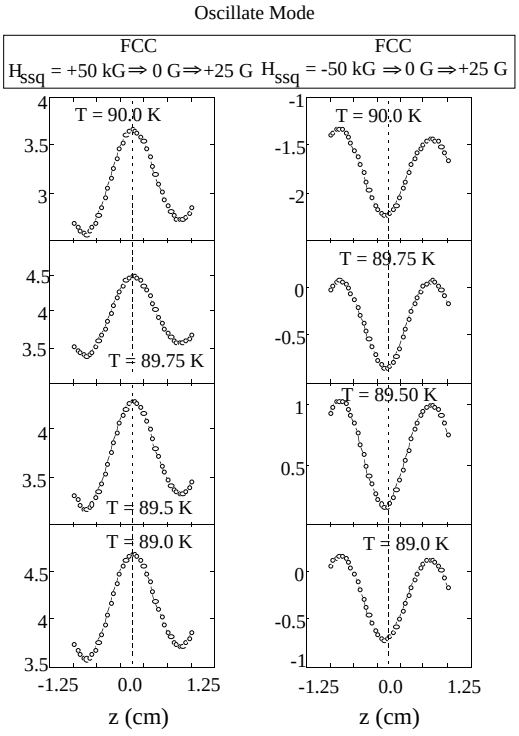

Figure D8(a). The SQUID output signals, V(z), near T_c for the FCC data shown in Figure D7.

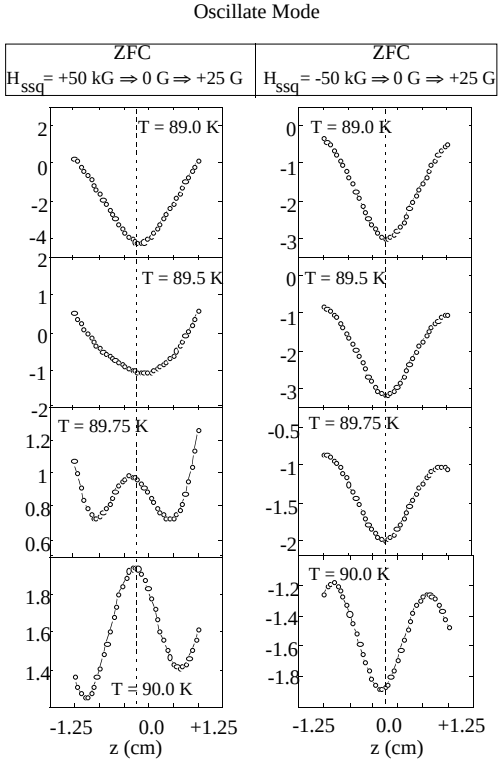

Figure D8(b). The SQUID output signals, V(z), near T_c for the ZFC data shown in Figure D7.

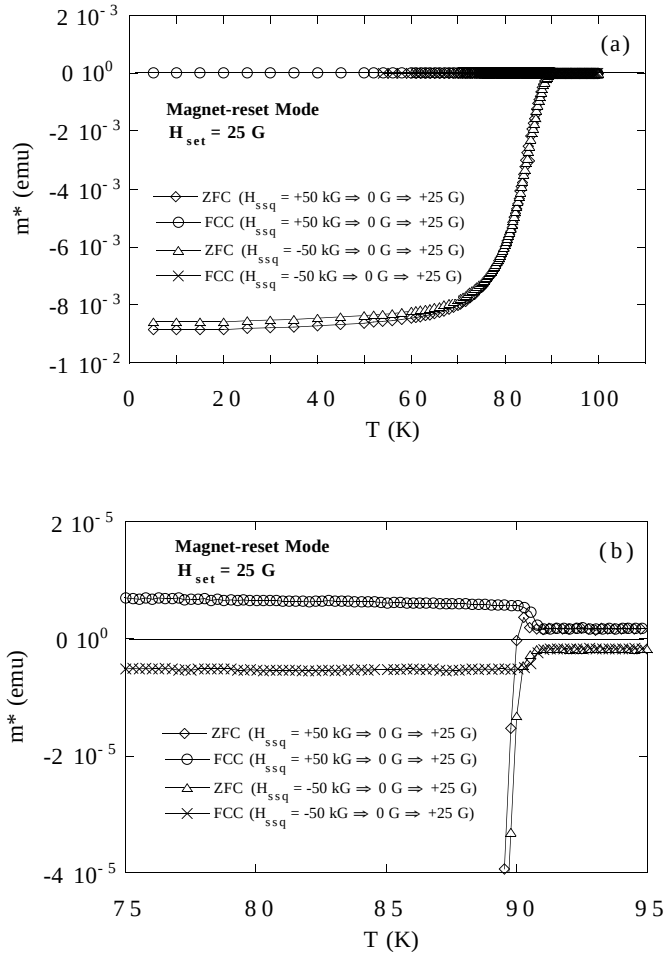

Figure D9. (a) ZFC- and FCC-m(T) curves measured at H_{set} = +25 G. H_{set} = 0 was set above T_c using the field-change sequences H_{ssq} = +50 kG ⇒ 0 G and H_{ssq} = -50 kG ⇒ 0 G using the magnet-reset option to set H_{set} = 0. The measuring field H_{set} = +25 G was applied at T = 5 K in the no-overshoot mode after zero-field cooling. (b) Expanded view of data near T_c.*

measurement of the magnetic moment of the sample within the error associated with the contribution from the non-uniformities.

It was shown in Section C that by using the oscillate mode to set H_{set} = 0 it was possible to reduce the H(z) curvature. Figure D7(a) shows the ZFC- and FCC-m*(T) curves measured at H_{set} = +25 G when the oscillate mode was used above T_c for the two field-change sequences H_{ssq} = +50 kG ⇒ 0 G and H_{ssq} = -50 kG ⇒ 0 G prior to setting H_{set} = +25 G at T = 5 K. [Figure D7(b) shows the same data in an expanded view in a narrow temperature range near T_c.] Figure C3 showed that when H_{set} = +25 G was set from these two conditions, the mirror symmetry observed about H = +25 for the no-overshoot mode was not observed. In particular there is a difference in the amplitude of the variations for the two H(z) curves. The effects of these differences are reflected in the m*(T) curves in Figure D7(b), which no longer exhibit the nearly perfect symmetry about m* = 0 that was observed for the no-overshoot mode. As is also evident in Figure D7(b), as a result of using the oscillate mode, the maximum in the ZFC- and FCC-m*(T) curves is located somewhat closer to T_c (89.7 K as compared to 89.1 K for the measurements made using the no-overshoot mode.) Note that the magnitude of m* for the pair of extrema in the FCC-m*(T) curves is about 1 x 10^{-5} emu when the oscillate mode is used, compared to m* values of nearly 1 x 10^{-4} emu for the same sample using the no-overshoot mode. This is entirely consistent with our previous observation that the field uniformity following an oscillate mode change is about a factor of 10 more uniform than when using the no-overshoot mode. Thus, the oscillate mode can produce a nearly ten-fold reduction in the magnitude of the apparent moments associated with field non-uniformities. Figures D8(a) and D8(b) show the FCC- and ZFC-V(z) curves for several temperatures near T_c for the data shown in Figure D7(b).

It was also shown in Section C that the field non-uniformities could be reduced even further by using the magnet-reset option. Figure D9(a) shows the ZFC- and FCC-m*(T) curves measured at H_{set} = 25 G, for the two field-change sequences H_{ssq} = +50 kG ⇒ 0 G and H_{ssq} = -50 kG ⇒ 0 G set using the reset option. [Figure D9(b) shows the same data in an expanded view in a narrow temperature range near T_c.] As shown in Figure C4, both H_{set} = +25 G curves have the same shape and amplitude variation, and the curves vary by less than 0.1 G between z = -2.5 cm and 2.5 cm, with larger (~ 0.1 G) deviations for $|z|$ > 2.5 cm. The similarity of the H(z) curves is reflected in the m*(T) curves in Figure D9(b), which again show the high degree of symmetry about m* = 0 similar to that observed for the no-overshoot mode. It is also evident that the maxima in the ZFC- and FCC-m*(T) curves are now located very close to T_c. The m* values for the extremum in the FCC-m*(T) curves are further reduced, having an apparent magnitude of about 5 x 10^{-6} emu, compared to an apparent magnitude of about 1 x 10^{-5} emu for the oscillate mode and 1 x 10^{-4} emu for the no-overshoot mode. The sharp change in both ZFC and FCC curves so close to T_c argues for an onset of strong flux pinning very close to T_c. Figures D10(a) and D10(b) show the V(z) curves for several temperatures near T_c for the data shown in Figure D9(b).

E. Modeling the SQUID Signals Resulting from Field Non-Uniformities

In Section D it was shown that the low-field FCC-m*(T) data appear to be a result of the particular magnetic

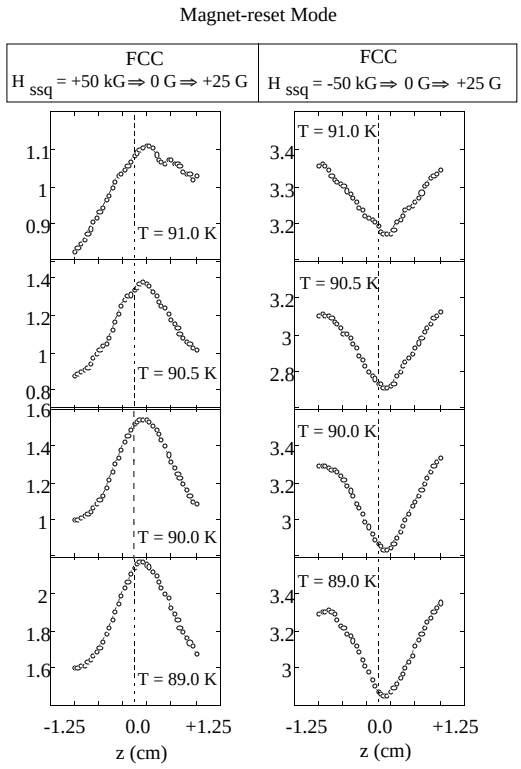

Figure D10(a). The SQUID output signals, V(z), near T_c for the FCC data shown in Figure D9.

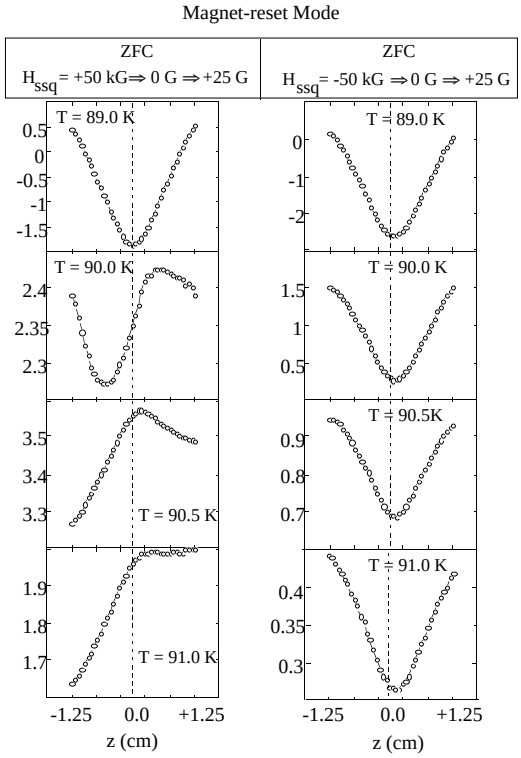

Figure D10(b). The SQUID output signals, V(z), near T_c for the ZFC data shown in Figure D9.

behavior of a superconductor moving through a non-uniform magnetic field, rather than a measurement of a constant magnetic moment. By merely setting the measuring field (H_{set} = +25 G) of the magnet using two different field-change sequences, two different FCC-m*(T) curves that are mirror images about m* = 0 were produced. The two sequences differ only in that one case involves setting H_{set} = 0 G from H_{set} = +50 kG, while in the second case H_{set} = 0 G was set from H_{set} = -50 kG. It was shown in Section C that these two field-change sequences generate H(z) profiles which are mirror images about H = +25 G (see Figure C2). Thus, the mirror symmetry of the FCC-m*(T) curves about m* = 0 is not at all surprising when the effects of the field non-uniformities on the V(z) SQUID signals are considered.

As discussed in Section D, near T_c the ZFC-m*(T) behavior also appears to be dominated by a magnetic response associated with the field non-uniformities. It is interesting to see how the systematic reduction in the field non-uniformity, by using the oscillate mode and then the magnet-reset option, leads to a reduction in the temperature range below T_c for which artifacts appear to dominate the ZFC behavior.

By considering accepted models of superconductor behavior, and using the experimentally measured H(z) profiles, it should be possible to account for the observed magnetic responses.[8,9] The very large differences between ZFC- and FCC-m*(T) curves observed under the most uniform field conditions (using the magnet reset option) suggest that strong-pinning effects completely dominate very close to T_c. This indicates that the Bean Critical State model should be applicable to the observed behavior, at least in the cases where the field non-uniformity is large enough to produce significant flux gradient penetration and where J_c is large enough to produce significant magnetic moments.

Using the Bean Critical State model, calculations of the expected SQUID output signals, V(z), and the position dependence of the true magnetic moment m(z), that are generated as the superconductor is transported through a non-uniform field, were made for a wide range of J_c values (see Appendix A for more details). (Reference 9 is a more realistic calculation that incorporates demagnetization effects.) Examples of the results of calculations for large, intermediate, and small J_c values (relative to the applied field) are shown in Figure E1. A second-order-polynomial fit to the measured H(z) profiles shown in Figure C2 was used for the calculations in Figure E1, with the H(z) curve displaced using an additive constant so that $m(z)$ had the initial value m = 0 at the point where transport through the detection coil and the non-uniform field would begin (z = -3). The H(z) curve models the transport of the sample

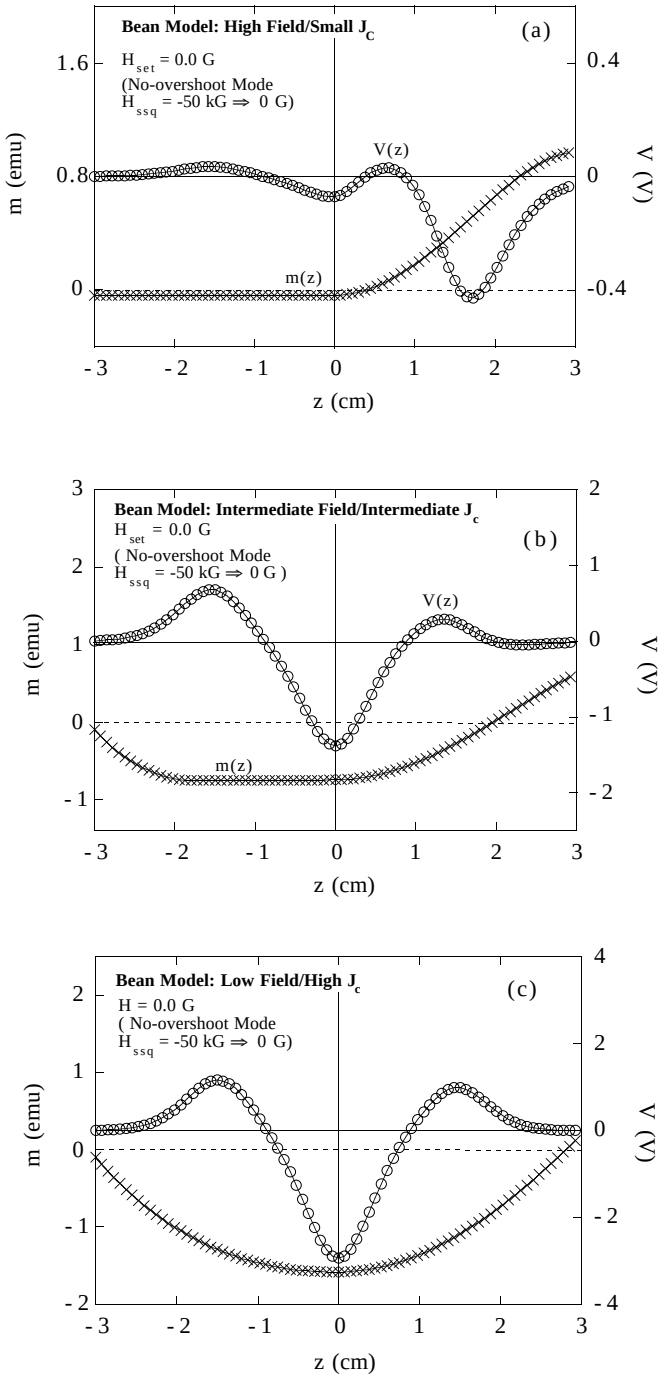

Figure E1. Calculations of m(z) and V(z) based on the Bean Critical State model in which the value m = 0 was used at the start of the measuring cycle (z = -3 cm). The experimentally measured H(z), following the H_{ssq} = 50 kG ⇒ 0 G sequence in the no-overshoot mode, was used in the calculation. (a) A very small J_c value was used in which case the critical state is attained with only a small field change (close to z = -3). (b) An intermediate value of J_c in which case the critical state is reached after more than 1 cm of travel. (c) A large J_c value in which case the critical state is not attained over the full field excursion experienced during the measurement.

from H = 0 through positive field values. It can be seen in Figure E1(a) that, for the case of small J_c values, the small field increase that occurs shortly after the sample begins the transport process is capable of driving the sample into the critical state [i.e., *m(z)* becomes a constant after a small field change]. In this case, as the sample passes the center (z = 0) the field decreases and then *m(z)* increases, with *m(z)* actually attaining a positive value by the end of its travel. The convoluted shape of the associated SQUID output signal, V(z), is also shown in Figure E1(a). The behavior of *m*(z) and V(z) are shown in Figure E1(b) for intermediate J_c values and in Figure E1(c) for large J_c values. For the intermediate J_c value chosen here, the critical state is reached closer to the center of the travel while in the large J_c case, the field non-uniformities are not large enough for the sample to reach the critical state and *m* changes continuously during transport. In all cases for the H(z) profile used, the sample has a positive moment by the end of its travel (at z = 3.0 cm).

To account for the observed behavior it is useful to consider the effects expected when a strong-pinning superconductor is cycled through a small *m*(H) loop. In the present case, the changes in H occur when the sample is moved through the non-uniform field during a measurement. The M(H) behavior for a strong-pinning superconductor is shown schematically in Figure E2. Cycling a strong-pinning superconductor up and down in field from H = 0 [through half an M(H) loop] leaves the superconductor in a remanent state, and cycling to positive field values will leave the superconductor in a remanent state with a positive magnetic moment (or magnetization). This effect was pointed out in the Bean-model calculations shown in Figure E1, where an excursion to positive fields due to the particular H(z) profile produces a positive magnetic moment which is evident as the positive *m* value at the end of the travel. Very close to T_c, J_c is very small and a significant remanent magnetization is not likely to be produced. However as J_c increases with decreasing temperature, cycling the sample in the non-uniform field should produce a significant remanent magnetization, particularly when the field non-uniformities are large.

The calculations shown in Figure E1 and the schematic of the Bean model in Figure E2, suggest that after one measuring cycle the sample should actually have a remanent magnetization prior to the beginning of the sample's next cycle. Within the Bean model there is a limit on the size of this remanent magnetization. When the sample begins moving to positive (increasing) fields — as when H_{ssq} = -50 kG ⇒ 0 G is used but with a positive remanent magnetization (at z = -3.0 cm) — the true magnetic moment will gradually decrease, cross through *m* = 0, and become negative, reaching a minimum at the position of largest positive field value (usually at the

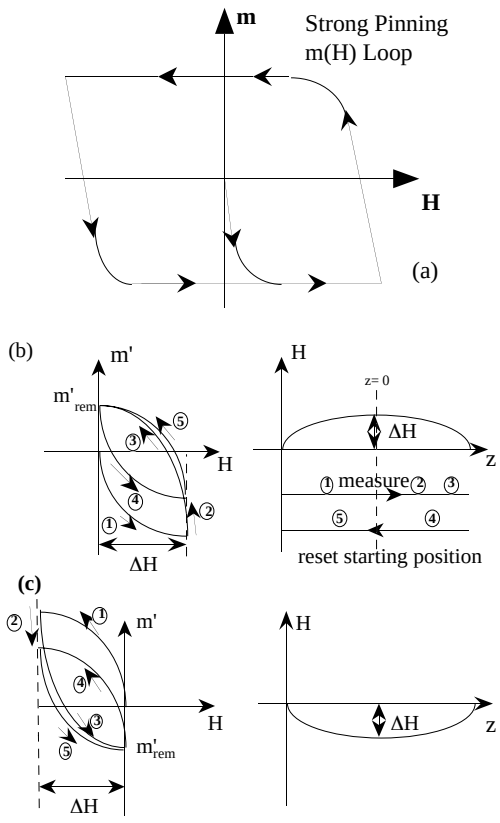

Figure E2. (a) A magnetic moment as a function of applied magnetic field curve for a sample exhibiting ideal Bean-Critical-State-model behavior. (b) The effects on magnetic moment resulting from cycling the sample through the non-uniform magnetic field. In this case the H(z) profile results in the cycling of the sample to positive field values leaving the sample with a positive remanent magnetization. The sample follows the reverse path as it is returned to the starting position. Data is collected only on the initial path. (c) In this case the H(z) profile results in the cycling of the sample to negative field values leaving the sample with a negative remanent magnetization.

center, $z = 0$). After passing the field maximum, the true magnetic moment will become more positive, finally returning to its positive starting value. An $m(z)$ curve exhibiting this behavior is shown in Figure E3(a). A computer fit to this V(z) signal would return a negative value for the magnetic moment. Thus, the "apparent" effect of flux pinning produced by field non-uniformities (when the field excursions initially move the sample to more positive fields) would be to produce a negative apparent magnetization. This should be the case no matter how large J_c becomes. This sequence was used for the FCC-m*(T) data shown in Figures D5, D7, and D9. Thus, it can be seen that in all cases the apparent magnetization becomes negative just below T_c, and in the case when the reset option was used, m* stays negative down to the lowest

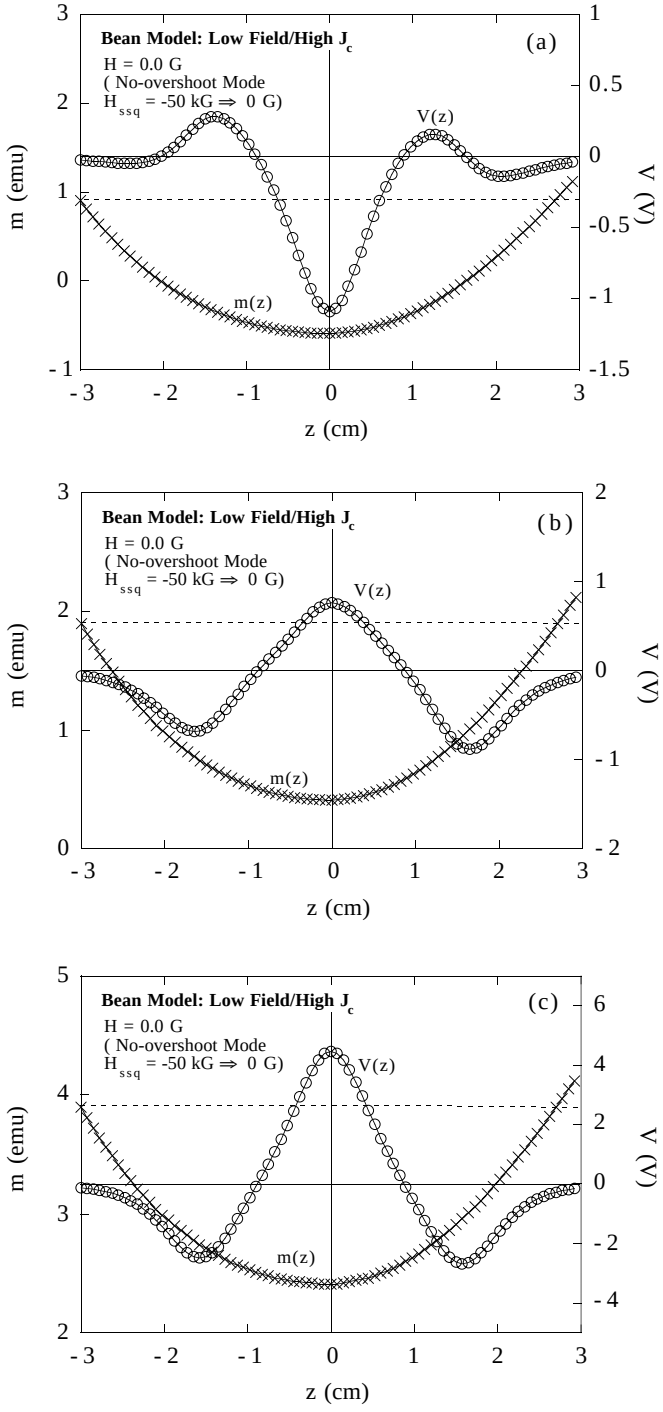

Figure E3. Bean model calculations similar to those of Figure E1 except that the magnetic moment at the start of a scan (z = -3) is not zero. From (a) to (c) the initial m value increases showing that the shape of the V(z) curve evolves from one that would produce a negative apparent magnetic moment m value, (a) when there is a small initial m value, to one that would produce a positive apparent magnetic moment m* value, (c) when there is a larger initial m value. This scenario is not supported by present Bean model calculations, even those which include demagnetization effects.*

temperatures. However, the FCC-*m** data for the oscillate and no-overshoot modes reverse sign at lower temperatures.

Figure E3(b) and E3(c) show calculations that demonstrate what could happen if the remanent magnetization could increase beyond the expectations of the Bean model. With increasing remanent magnetization at the beginning of the sample's travel, the V(*z*) signal evolves from what initially would produce a negative apparent moment *m** using a computer fit [Figure E3(a)], into a signal that would produce a positive apparent moment *m** using a computer fit [Figure E3(c)]. Unfortunately, even though this scenario (of larger and larger remanent magnetization values) could explain the observations there is no apparent reason why the remanent magnetization should increase beyond the expectations of the Bean model. Thus, we presently have no explanation for the reversal in sign of the FCC-*m**(T) curves that is observed when the no-overshoot or oscillate modes are used prior to setting the measuring.

At some point below T_c, the effects of field non-uniformities will no longer dominate the ZFC-*m**(T) data. The crossover from artifact dominated *m** values to more quantitatively-accurate magnetic-moment values occurs closer to T_c as the field uniformity increases. When using our particular sample in the specific geometry chosen, the magnitude of V(*z*) generated by field non-uniformities when the no-overshoot mode is used, is comparable to the V(*z*) signal generated by a sample with a dipole-moment of about 2.5×10^{-4} emu, while for the oscillate mode it compares with a moment of about 1.5×10^{-4} emu. For the magnet reset option, the V(*z*) associated with field non-uniformities is comparable to a moment of about 0.5×10^{-4} emu. For the ZFC-*m**(T) measurement, the sample has an *m** magnitude of about 3.5×10^{-2} emu at the lowest temperatures and this gradually decreases with increasing temperature. The crossover from accurate magnetic moment data to artifact-dominated data occurs approximately at the point where the ZFC-*m**(T) curves associated with the two different field-change sequences split. For the no-overshoot data this occurs at a temperature of about 84.2 K, where the apparent magnetic moment *m** has a magnitude of about -3×10^{-3} emu. For the oscillate mode the split occurs at $T \approx 89.5$ K (and $m^* \approx 4 \times 10^{-5}$ emu) while there is no evidence of a split for the data collected after using the magnet reset option.

For those cases in which temperature is the parameter of importance (e.g., T_c) it is possible to use the appearance of non-dipole V(*z*) signals to make very accurate determinations of the characteristic temperature as suggested by Suenaga et al.[3] We have determined J_c to the resolution of the 0.25 K temperature steps using the appearance of non-dipole V(*z*) signals. Remarkably, the larger the non-uniformity of the field, the larger will be the non-dipole signals produced, so that when determining a characteristic temperature one may actually take advantage of data which might otherwise be regarded as a "problem" or artifact. The V(*z*) signal is always a legitimate measurement of the magnetic response. The appropriate analysis of the output signal can provide valuable quantitative magnetic information.

F. Effects of Field Non-Uniformities in Large Applied Fields

As the magnetic field is increased, the onset of irreversible magnetic behavior at the vortex-solid phase transition T_g moves to lower temperatures. The combination of ZFC- and FCC-*m**(T) measurements has become a standard method for identifying the onset of irreversibilities at T_g. This method exploits the history dependence associated with irreversible behavior, since as mentioned earlier, the observed M value depends on the particular sequence of field and temperature changes that brought it to its present state. The temperature range over which the ZFC- and FCC-*m**(T) curves are separated corresponds to the region of (strong) pinning, and therefore irreversible behavior, while the temperature range over which the curves are superimposed usually corresponds to reversible behavior.

The application of a large field can lead to some additional complications. What had been a very small background contribution in small fields can now become a significant contribution to the signal. An extreme example of this effect is a thin superconducting film on a relatively thick substrate. The very small mass of superconducting material — in the present case there is about 5 micrograms (5×10^{-6} g) of superconductor on a substrate with a mass of 34 milligrams (34×10^{-3} g) — means that above T_g the signal can be strongly dominated by the substrate. If the J_c of the film is large enough, the superconductor's magnetization will dominate at some temperature below T_g, and the larger the value of J_c, the closer in temperature to T_g it will dominate. (While a diamagnetic superconducting response is expected between the vortex-solid transition and H_{c2}, this signal is usually too small to observe experimentally for a thin film sample.) The same considerations exist for crystals and bulk samples as for thin films, with the relative magnitudes of the background and sample signal determining how important the background contribution will be.

When the contributions of the background and sample are of comparable magnitude, it is often not a simple matter to subtract out the background contribution. A further problem arises when the center-of-mass of the sample and the center-of-mass of the background are displaced

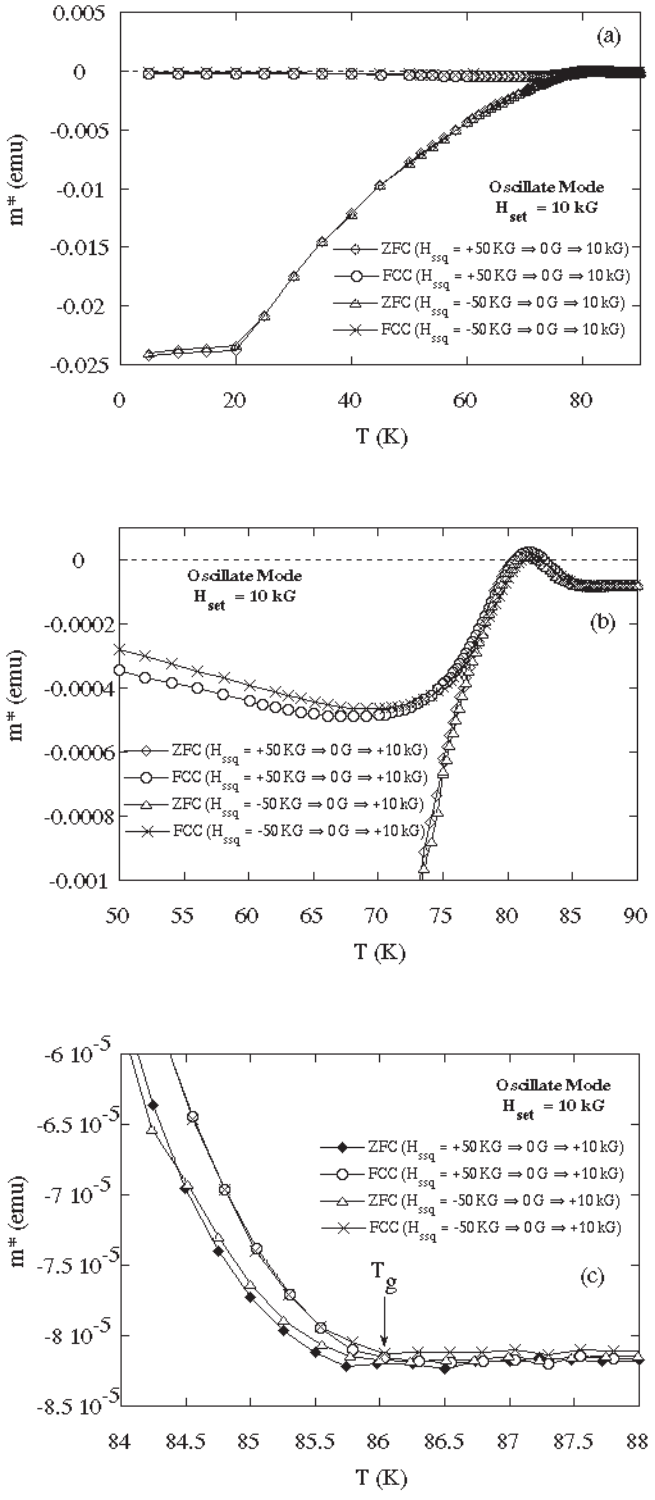

Figure F1. ZFC- and FCC-m(T) curves measured at H_{set} = +10 kG. H_{set} = 0 was set above T_c using the field-change sequences H_{ssq} = +50 kG ⇒ 0 G and H_{ssq} = -50 kG ⇒ 0 G in the oscillate mode, while the measuring field H_{set} = +10 kG was applied at T = 5 K using the no-overshoot mode after zero-field cooling. (a) Measurements over the full temperature range, (b) on expanded x and y scales, and (c) near T_g.*

spatially (primarily along *z*). This is a problem for **all** kinds of magnetometer measurements, not just for SQUID magnetometer measurements made with the MPMS, since magnetometers are usually designed to determine the magnetic moment of samples that approximate point dipoles. (This issue was discussed at some length in the Quantum Design Application Note #1.) Another effect which can also complicate an otherwise straight-forward background correction is the fact that below T_c the screening of the superconductor can change the local magnetic field experienced by the background. Thus, measuring the background above T_g or in a separate measurement may not reflect its actual contribution below the T_g of the sample.

Figure F1(a) shows ZFC- and FCC-*m**(T) curves measured at H_{set} = +10 kG over the full temperature range studied. H_{set} = 0 was set above T_c using the field-change sequence H_{ssq} = +50 kG ⇒ 0 G or H_{ssq} = -50 kG ⇒ 0 G in the oscillate mode, while the measuring field H_{set} = +10 kG was applied at T = 5 K using the no-overshoot mode after zero-field cooling. On the scale in Figure F1(a) the FCC-*m**(T) data remains very close to zero, with some small features evident at higher temperatures. Figure F1(b) shows the same results with expanded scales. There are clearly differences between the data in which the H_{ssq} = +50 kG ⇒ 0 G sequence was used in the field preparation compared to the data in which H_{ssq} = -50 kG ⇒ 0 G was used. In Figure F1(b) it is much more evident how *m** increases just below T_g for both field-change sequences. This reflects an evolution of the H(*z*) profile at larger fields. Also more evident is the significant diamagnetic signal above T_g which has its dominant contribution from the substrate. Since the parameter of interest in the ZFC/FCC measurement is a characteristic temperature rather than a magnetization value, it is possible to use the changes in the V(*z*) signals to make very accurate determinations of the onset temperature for irreversible behavior.[3]

Figure F1(c) shows the same data near T_g with scales further expanded. The vortex-solid transition at T_g is identified in the figure as the point where the pairs of ZFC- and FCC-*m**(T) curves become superimposed. Because the signal in this case is so heavily dominated by the substrate there is no evidence of the equilibrium magnetization of the superconductor expected at temperatures between T_g and the temperature of the upper critical field, T_{c2}. The V(*z*) signals near T_g are shown in Figure F2 where it can be seen that there is a dramatic change in the shape of the V(*z*) signal at T_g, with constant-dipole curves above $T_g \approx 85$ K and extremely anomalous curves below T_g. Figure F3 shows the V(*z*) signals associated with the data in Figure F1 over a larger range of temperatures.

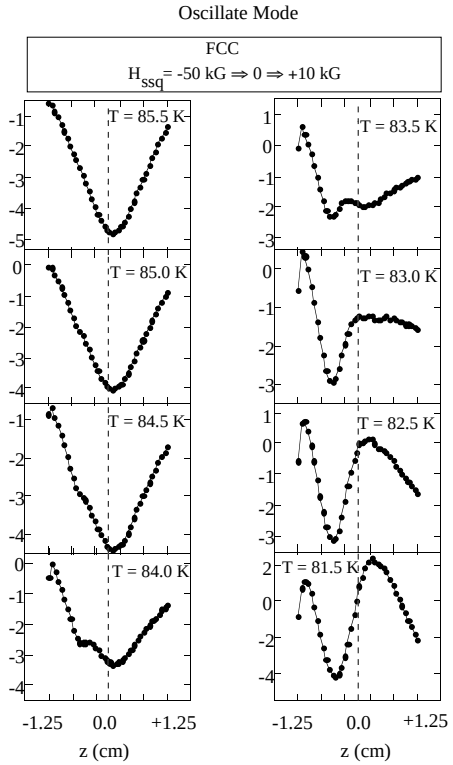

Figure F2. The V(z) signals near T_g for the FCC data shown in Figure F1.

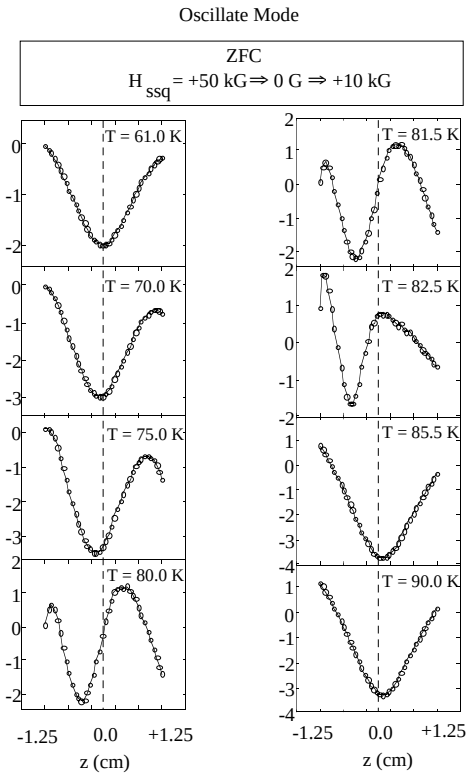

Figure F3(a). Some of the SQUID output signals V(z) associated with the ZFC data shown in Figure F1.

The ZFC- and FCC-*m**(T) curves measured at H_{set} = +10 kG — when the no-overshoot mode was used during the field-change sequences H_{ssq} = +50 kG ⇒ 0 G and H_{ssq} = -50 kG ⇒ 0 G — are shown in Figure F4. These curves are slightly different than those observed for the oscillate mode, and a brief examination of Figure F1(c) and F4(c) show that it is easier to determine the temperature of the transition, T_g, when the less uniform field is used. In Figure F4(c) there is a clear departure from the four superimposed curves at a temperature of 86 K.

The H(*z*) profiles in Figure F5 show how H(*z*) evolves as H_{set} increases from +1 kG to +5 kG. The associated FCC-*m*(z)* curves are shown in Figure F6. It can be seen that for the curves in which H_{ssq} = +50 kG ⇒ 0 G was used, the H(*z*) profiles evolve from having a minimum near *z* = 0, into an asymmetrical curve (with respect to *z* = 0) with a minimum, and finally into curves with a maximum near *z* = 0. On the other hand, the H(*z*) curves for which H_{ssq} = -50 kG ⇒ 0 G was used, always have a maximum near *z* = 0, thus the H(*z*) profile with a maximum near *z* = 0 is characteristic of increasing H with a change of about 5 kG required to reverse the H(*z*) profile (for a magnet state produced under these particular conditions). The evolution of the H(*z*) profiles is reflected in the FCC-*m*(z)* data in Figure F6 where the curves associated with H_{ssq} = +50 kG ⇒ 0 G become more positive and progressively approach

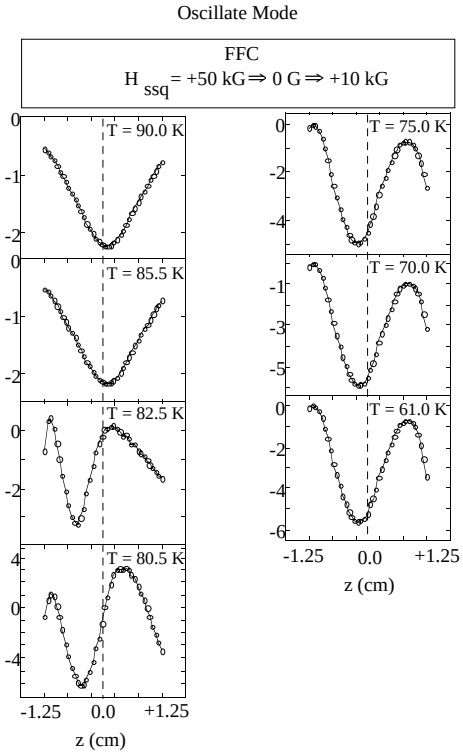

Figure F3(b). Some of the SQUID output signals V(z) associated with the FCC data shown in Figure F1.

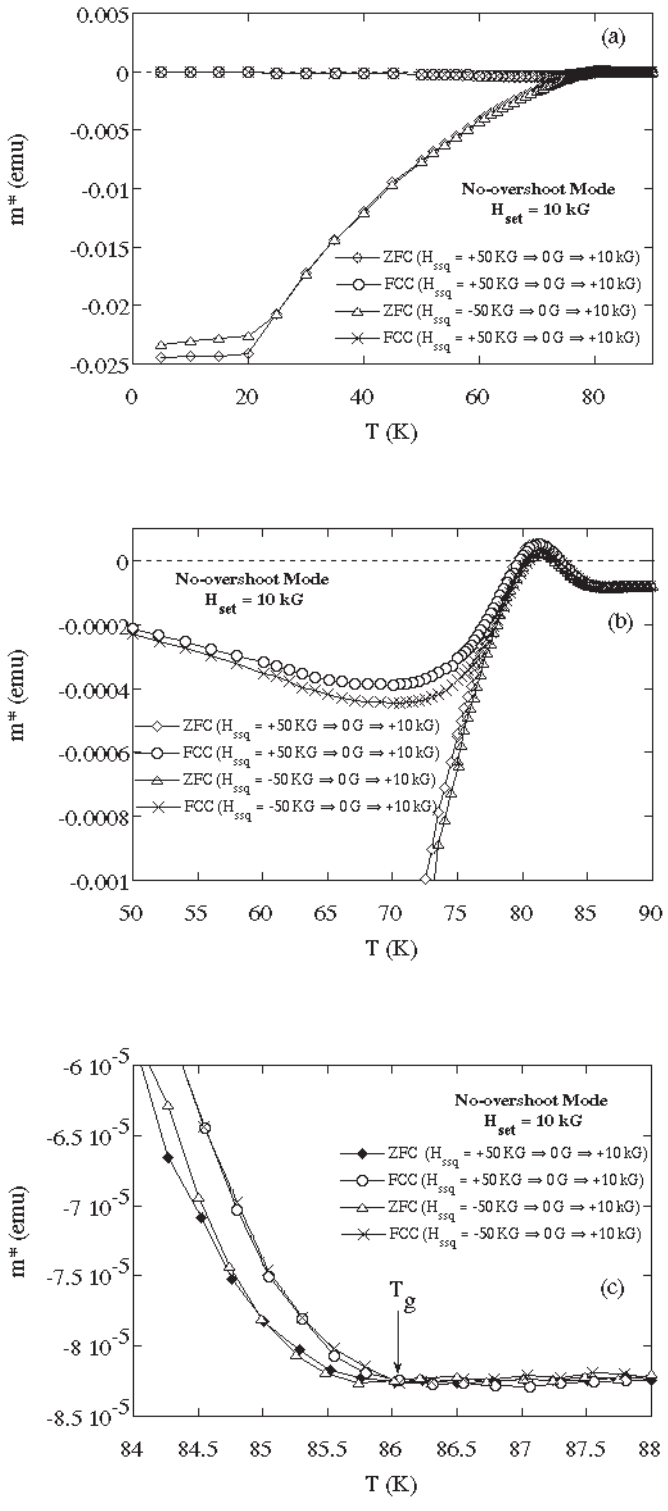

Figure F4. ZFC- and FCC-m(T) curves measured at H_{set} = +10 kG. H_{set} = 0 was set above T_c using the field-change sequences H_{ssq} = +50 kG ⇒ 0 G and H_{ssq} = -50 kG ⇒ 0 G in the no-overshoot mode, while the measuring field H_{set} = +10 kG was applied at T = 5 K in the no-overshoot mode after zero-field cooling. a) Measurements over the full temperature range, b) on expanded x and y scales, and c) near T_g.*

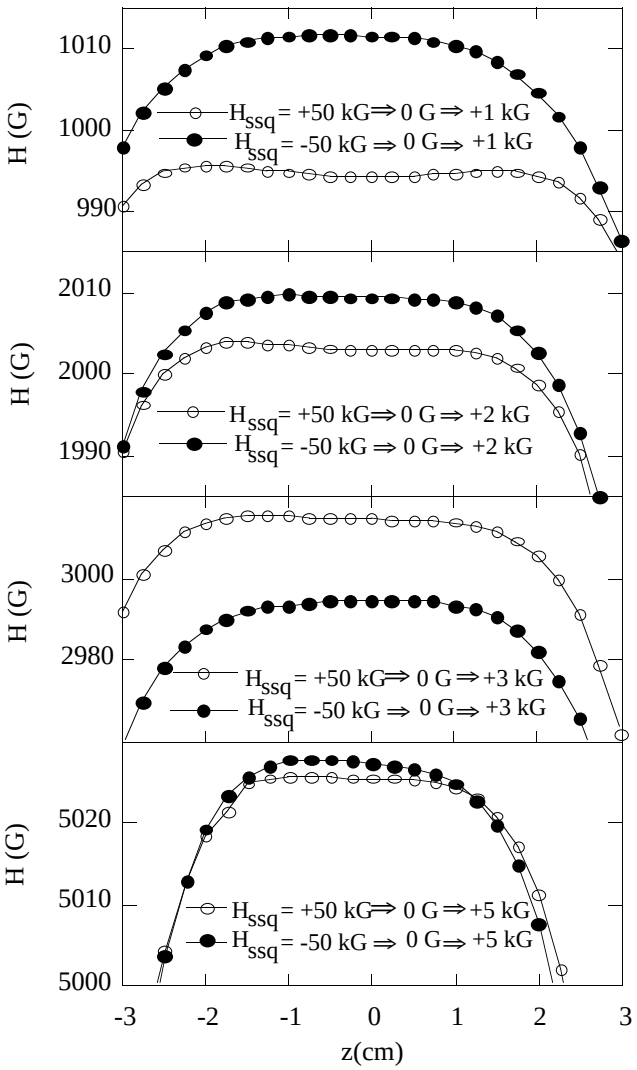

Figure F5. The H(z) profiles produced using the no-overshoot mode as measured using a Hall-effect device, evolve in shape as the magnetic field value is increased. For the case when H_{ssq} = -50 kG ⇒ 0 G is used to set the initial field, the field retains a maximum at the center (z = 0), whereas when H_{ssq} = +50 kG ⇒ 0 G is used, there is an evolution from a minimum to a maximum as the field increases to H_{set} = +5 kG.

the shape of the curves associated with the sequence H_{ssq} = -50 kG ⇒ 0 G as the field increases to +5 kG.

When the V(z) signals deviate significantly from a constant-dipole response some rather unusual effects can be observed in the behavior of the apparent magnetic moment. For example, the results in Figure F7 show large discontinuities in the *m**(T) curves when the *iterative regression* method (rather than the linear regression method used in this study) was used to analyze the V(z) results. In fact, there is a factor of about 1.6 between the values of *m** above and below the discontinuities.

Repeating the signal analysis using the linear regression method produces *m**(T) curves without discontinuities. The discontinuities are associated with a change in the analysis method during the measurement. The computer software places limits on the errors associated with the iterative regression fit, and when this error is exceeded the system will repeat the signal analysis using the linear regression method. Since the signal is not a dipole-like response, the different algorithms used in the different fit routines can produce rather different apparent magnetic moments *m**. For this reason, in this study the linear regression routine was used to generate all of the *m**(T) curves other than those in Figure F7.

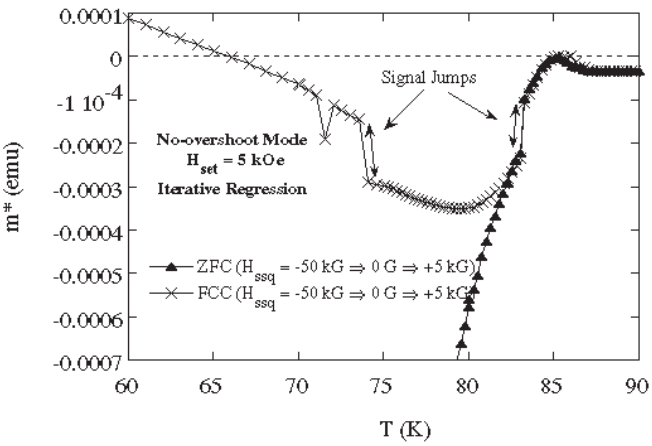

Figure F7. ZFC- and FCC-m(T) curves measured at H_{set} = +10 kG. H_{set} = 0 was set above T_c using the field-change sequence H_{ssq} = +50 kG ⇒ 0 G in the no-overshoot mode, while the measuring field was applied at T = 5 K after zero-field cooling. The discontinuities are associated with a change in the computer analysis method during the measurement, when a large error is encountered in the iterative regression algorithm.*

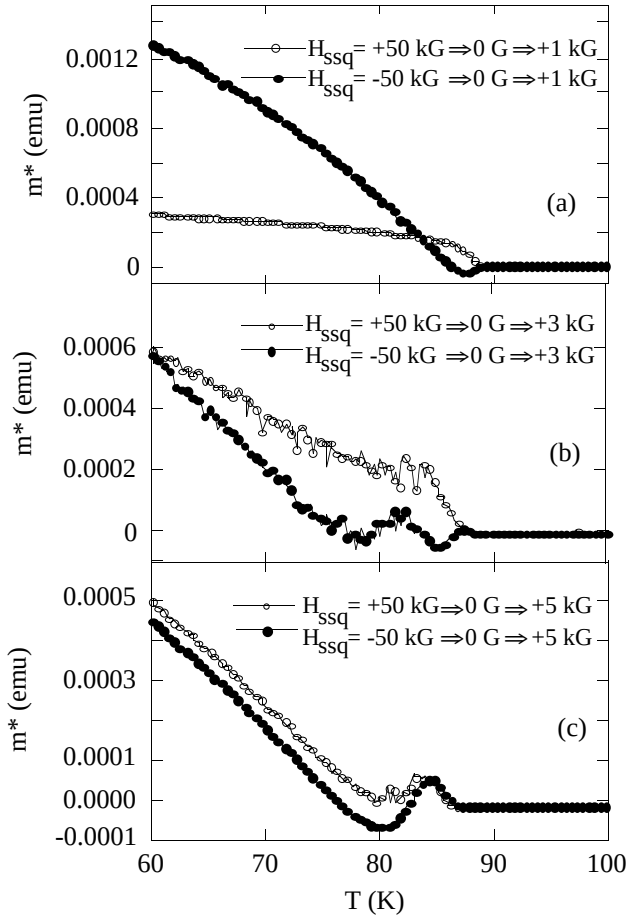

Figure F6. The evolution of the H(z) profiles shown in Figure F5 lead to a related evolution in the FCC-m(T) behavior near the vortex-solid phase transition at T_g. In 1 kG (a) the FCC-m*(T) curve associated with H_{ssq} = +50 kG ⇒ 0 G takes on more positive values and by H_{set} = +5 kG (c) the two FCC-m*(T) curves exhibit nearly the same behavior.*

G. Implications of Anomalous Signals for Magnetization Measurements

Most of the problems described here have a very long history that dates back far beyond the appearance of the MPMS or any other SQUID magnetometer. When a sample and its background do **not** approximate a constant, point dipole, complications can arise with any magnetometer. Field uniformity is always a problem that can be reduced by shortening the sample travel-length during measurement or by improving the properties of the magnet. The MPMS incorporates a high-uniformity superconducting magnet, but in addition there are features designed to accommodate a reasonably short scan length and, as shown, several field-change methods available for improving the field uniformity.

Since there are limits to how much improvement can, or should, take place in automated signal analysis, it is important for the scientist to understand the potential pitfalls in the measurements they are making. It is also important to know exactly what property (quantity) one wishes to measure in order to decide if the data will be suitable. For example, the values of *m** reported by the MPMS using computer fit routines, for temperatures very close to T_c and T_g, are clearly not accurate determinations of the true magnetic moment *m* of the sample. However, in the particular case presented here, the ZFC/FCC method can still provide a very accurate determination of the transition temperatures T_g and T_c. In fact, some of the "problems" associated with field non-uniformity discussed

here may actually enhance the accuracy of measuring these characteristic temperatures.

ZFC-m^*(T) and m^*(H) data can also be used to provide an accurate measurement of certain properties including J_c when the signal associated with the trapped flux is much larger than the signal associated with field non-uniformities. The FCC-m^*(T) measurement, on the other hand, is very often misunderstood and misused. The FCC-m^*(T) measurement has been used to measure the *superconducting fraction* and is occasionally used to measure J_c. In neither case is the FCC measurement generally reliable due to the effects of flux pinning. This is because flux is not readily expelled from a strong-pinning superconductor as it is lowered in temperature in a field smaller than H_{c1}. For determining J_c, the most reliable magnetic method is probably an M(H) [m^*(H)] measurement. The virgin curve — the initial part of a zero-field-cooled M(H) curve — can be useful for determining the superconducting fraction, however it must be properly corrected for demagnetization effects.

Some of the SQUID output signals, V(*z*), shown in earlier sections look similar to an ideal dipole signal even though the origin of the signal is completely spurious. Computer fits to these signals can return what appear to be reasonable values of the magnetic moment and even give small error values for the regression fit. Caution must be exercised when interpreting results of this kind since, as has been shown, such results are sometimes not dipole response curves with slight deviations, but rather are the responses associated with a completely different kind of magnetic behavior. Problems will result from the imprudent use of analysis methods meant for extracting a magnetic moment, however, with the appropriate choice of analytical method valuable magnetic information can be extracted from the measurements in all cases.

As mentioned earlier, when the contribution of the background and sample are of comparable magnitude, and when the center-of-mass of the sample and the center-of-mass of the background are spatially displaced, significant deviations from constant-dipole V(*z*) signals can result. In some of these cases it is possible to measure the V(*z*) signals of the background separately at the same fields and temperatures at which the V(*z*) signals of the combined sample and background are measured. It is preferable for the background to be located in exactly the same position in both runs. The V(*z*) signals from the two runs can then be subtracted to produce a set of V(*z*) curves that represent the response of the sample alone. An application of this method is shown in Figure G1.

It must be emphasized that the effects that have been described here are not unique to any specific magnetometer, and are not even unique to SQUID magnetometer systems. While the measurements described in this document were all performed on the Quantum Design MPMS SQUID magnetometer system, any magnetometer measurement in which the sample experiences variations in the magnetic field during the measurement process will be subject to similar effects. One might argue that the effects could be eliminated by

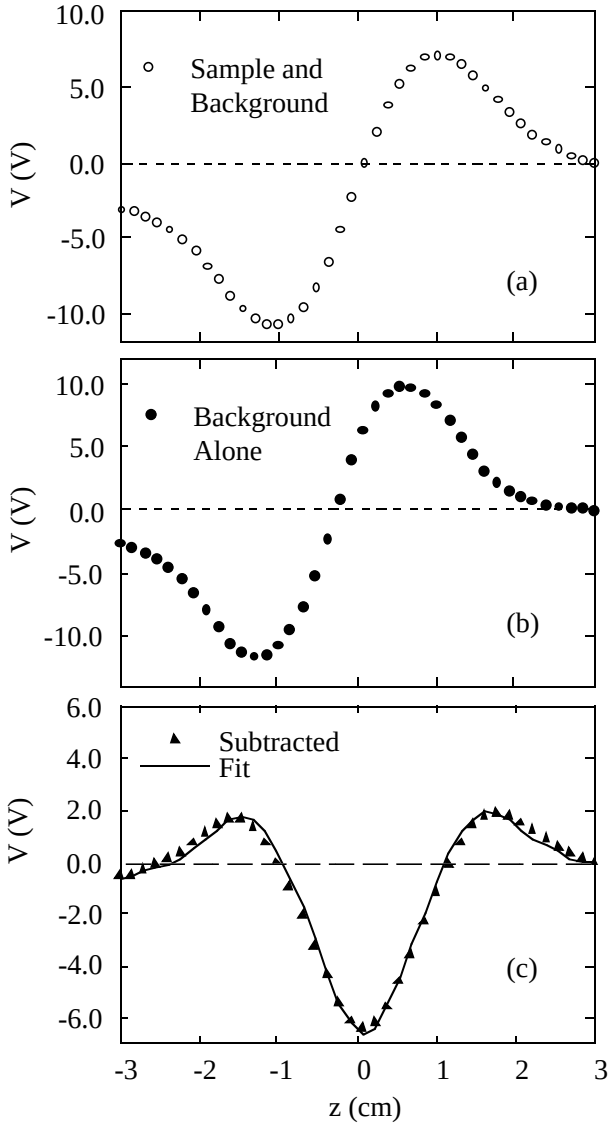

Figure G1. In some cases the sample with background does not approximate a magnetic dipole and will produce a V(z) response for which the signal analysis routines included with the MPMS are not applicable. By collecting the V(z) curves for (a) the sample with background and then (b) the V(z) for the background alone, at each of the fields and temperatures of interest, one can then subtract corresponding V(z) curves to produce the V(z) curve for the sample alone. Analysis is made easier by locating the background in exactly the same position during both runs.

just providing a more uniform magnetic field. However, in the case of measurements made at very low fields, and because of flux trapping effects in superconducting magnets, this may not be possible within reasonable cost and size constraints for any practical system containing a high-field superconducting magnet.

Acknowledgements

We would like to thank Minoru Suzuki of Nippon Telegraph and Telephone and Jim Thompson of Oak Ridge and University of Tennessee for very important insights. We would also like to thank Jost Diederichs of QD for offering critical comments and Lifang Hou for preparing and patterning the YBCO thin film. Many helpful comments were provided by Ron Goldfarb of the National Bureau of Standards and Technology in Boulder, Colorado. Refereed journal publication of some portions of this text are in preparation with John R. Clem of Iowa State University and Alvaro Sanchez of Universitat Autonoma de Barcelona who have made detailed, realistic theoretical calculations of the effects of the measuring processes discussed here. Some support for this work was provided by the Director for Energy Research, Office of Basic Energy Sciences through the Midwest Superconductivity Consortium (MISCON) grant #DE-FG02-90ER45427.

References

1. D. Farrell, in *Physical Properties of High Temperature Superconductors, IV*, edited by Don Ginsberg (World Scientific, 1989), pp. 49-53.

2. C. P. Bean, Rev. Mod. Phys. 36, 31 (1964).

3. M. Suenaga, D. O. Welch, and R. Budhani, Supercond. Sci. Technol. 5, s1 (1991).

4. A. K. Grover, Ravi Kumar, S. K. Malik, and P. Chaddah, Solid State Comm. 77, 723 (1991).

5. F. J. Blunt, A. R. Perry, A. M. Campbell, and R.S. Liu, Physica C 175, 539-544 (1991).

6. Minoru Suzuki, Kazunori Miyahara, Shugo Kubo, Shin-ichi Karimoto, Koji Tsuru, and Keiichi Tanabe. (preprint)

7. M. McElfresh, *Fundamentals of Magnetism and Magnetic Measurements featuring Quantum Design's Magnetic Property Measurement System*, (Quantum Design, San Diego, CA, 1994).

8. S. Libbrecht, E. Osquiguil, and Y. Bruynseraede, Physica C 225, 337 (1994).

9. Shi Li, Lifang Hou, and M. McElfresh, John R. Clem, and Alvaro Sanchez, (preprint).

Appendix A: Introduction to the Bean Critical State Model

The Bean Critical State model is used to relate the critical current density J_c, which is the largest possible supercurrent (zero-dissipation or zero-resistance current), to the total magnetization of a type-II superconductor for the particular case in which J_c is limited by flux pinning. The model relates the magnetization M to J_c by the simple formula $J_c = sM/d$, where *d* is the sample width or diameter and the constant *s* is a shape dependent constant having a value $s = 10/\pi$ for a slab sample and $s = 15/\pi$ for a cylindrical sample. Several assumptions are usually made when using the Bean model. For instance, it is usually assumed that the lower critical field H_{c1} is very small (it is usually ignored) and a key assumption is that the current density J in the sample can have only the values $+J_c$, $-J_c$, or zero. The simplest version of the model treats the case of an infinitely long sample in a parallel field such that demagnetization effects are not important.

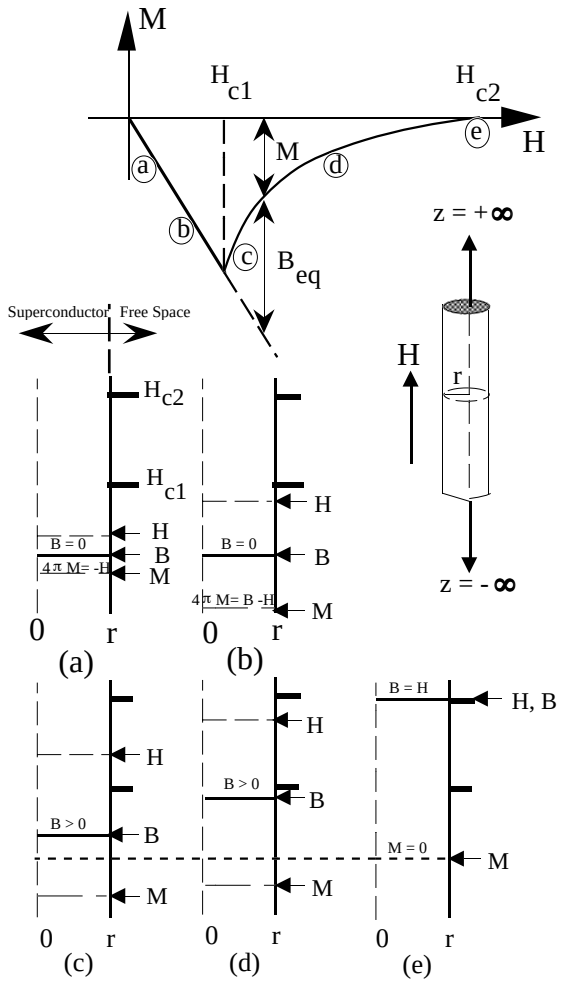

Figure APP-A1. Magnetization M as a function of applied field H for a long cylindrical sample of an ideal type-II superconductor in a parallel magnetic field. The plots in (a) through (e) compare the values of the applied field H, the magnetization M, and the flux density B inside the sample at various points on the M(H) curve. For an ideal superconductor, M, B, and H will all be uniform inside the sample.

The magnetization as a function of applied magnetic field M(H) for an ideal type-II superconductor (without flux pinning) is shown in Figure APP-A1. As the applied magnetic field is increased from H = 0, at temperatures below the superconducting transition temperature T_c, initially the superconductor completely screens out the magnetic field (B = 0 within the sample). When H reaches H_{c1} magnetic flux enters a type-II superconductor in the form of magnetic-flux quanta known as flux vortices. (One quantum of magnetic flux $\phi_0 = 2.07 \times 10^{-7}$ oersted-cm^2.) As H continues to increase, the vortex-solid transition boundary is crossed at H_g, at which point $J_c = 0$, and then the upper critical field H_{c2} is crossed, above which the sample is no longer superconducting (it becomes normal). The region $H_{c1} < H < H_{c2}$ is known as the vortex phase. A magnetic phase diagram is shown in Figure APP-A2. In contrast to this, a type-I superconductor fully screens up to the critical field, H_c, above which it becomes normal.

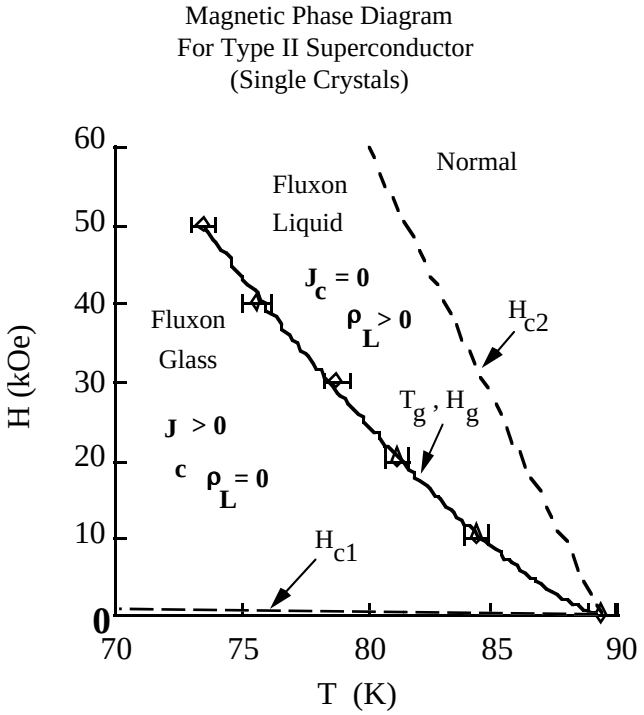

Figure APP-A2. Magnetic phase diagram for a type-II superconductor. The lower and upper critical fields, H_{c1} and H_{c2} respectively, have long been known whereas the vortex-solid transition boundary $H_g(T)$ is a more recent discovery.

A superconductor with an ideal-shaped M(H) loop like the one shown in Figure APP-A1 would not be able to support a supercurrent in the vortex phase. This is because the flux vortices are free to move in the sample and the application of a transport current will cause the vortices to experience a Lorentz force $\mathbf{F}_L = \mathbf{J} \times \boldsymbol{\phi}_0$, where **J** is the current density. The force will lead to motion of the vortices which will in turn generate a voltage parallel to **J** that results in dissipation of the supercurrent. In order to keep the vortices from moving, the vortices must be *pinned*. Pinning is produced by creating spatial variations in the properties of the superconductor, usually by introducing particular types of defects. The largest current density that a superconductor can support without dissipation is J_c. In the event that J_c is limited by flux-vortex motion, the J_c will be determined by the balancing of the Lorentz and pinning forces. There are other possible limits to J_c, such as the depairing limit which is usually two orders of magnitude larger than the largest J_c associated with flux pinning. Clearly the mechanism that produces the smallest value of J_c will determine the J_c of a given sample. In granular superconductors, J_c is often much lower than either the pinning-limited J_c or the depairing-limited J_c, limited instead by the superconducting weak-links at the grain boundaries.

Before discussing the Bean model further, it is useful to discuss the behavior of an ideal type-II superconductor (with no defects). Shown schematically in Figure APP-A1 is an infinitely long cylindrical sample. The magnetic field is applied parallel to the axis of the cylinder. As the field is applied supercurrents at the surface are produced to screen the interior of the cylinder in order to maintain B = 0 inside. For the case of an ideal type-II superconductor for $H < H_{c1}$, the currents would only exist near the surface in a thin layer in which the magnitude of the field decays into the sample with the characteristic length λ, the magnetic penetration depth. The B(r) profile associated with two representative values of the applied field less than H_{c1} are shown in Figs. APP-A1(a) and APP-A1(b), with the applied field H, the magnetization $4\pi M$, and the magnetic flux density B identified in the figures. It can be seen that as H increases (while still below H_{c1}), B remains at zero since the interior is completely screened, meaning that the screening currents produce a magnetization value, $-4\pi M$, that is equal and opposite to the applied field. When H exceeds H_{c1} [Figure APP-A1(c)] flux penetrates into the superconductor, and in the ideal case this flux is uniformly distributed within the sample. The magnitude of the magnetization is now reduced and the amount of flux penetrating the sample is proportional to the flux density B. The magnitude of M continues to decrease [Figure APP-A1(d)] until H = B at the upper critical field H_{c2} [Figure APP-A1(e)], which is where the sample becomes normal (non-superconducting). For an ideal superconductor the same curve is followed on decreasing applied field.

In contrast to the ideal superconductor in which a continuum of current values can exist, the Bean model assumes that only the current densities $\pm J_c$ and zero are possible, so that for a non-zero applied field H, the current density J_c always flows to some depth. As H increases, the depth to which this current (J_c) flows also increases. This is shown schematically for the simplest version of the Bean model in the series plots in Figure APP-A3, with the position dependence of the current shown in Figure APP-A3(a) and the position dependence of the amplitude of the magnetic flux density, B(r), shown in

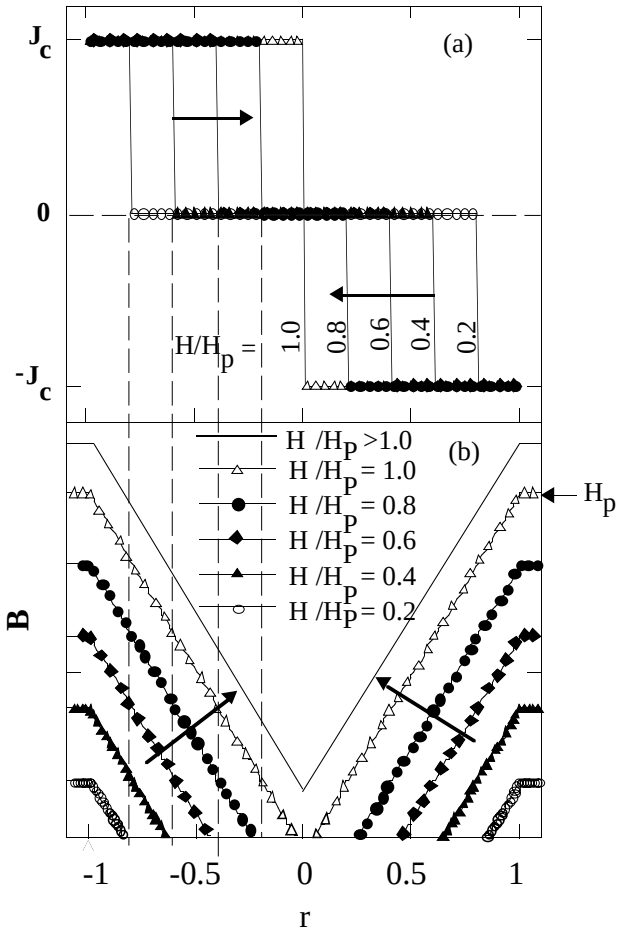

Figure APP-A3. (a) A calculation of the spatial dependence of the current and (b) the position dependence of the amplitude of the magnetic flux density B as described by the simplest version of the Bean Critical State model for a long cylindrical sample in a parallel field. Here r = 0 corresponds to the center (on the symmetry axis) of the sample and r = 1 corresponds to the sample surface. The only possible values of current density are $\pm J_c$ and zero, with $J = J_c$ flowing to the depth to which the flux penetrates and J = 0 where B = 0.

Figure APP-A3(b). Here r = 0 corresponds to the center (on the symmetry axis) of the sample and r = 1 corresponds to the sample surface. It can be seen that the magnetic flux density, B(r), decreases linearly from the surface, and for small applied fields the region near the axis of the sample is fully screened (B = 0). As the applied field increases, the depth to which flux penetrates also increases, and within the depth to which the flux penetrates, a current of magnitude J_c flows. At a sufficiently high field, labeled H_p (the penetration field), the flux fully penetrates to the center of the sample and the sample is now in the *critical state*, with $+J_c$ or $-J_c$ flowing throughout the sample. As the field continues to increase, flux continues to penetrate, however the slope dB/dx remains the same. In fact because $dB/dx \sim J_c$, and $J = \pm J_c$, within the Bean model the slope is always $\pm dB/dx$ inside the superconductor.

Figure APP-A4 shows an M(H) loop for the simplest case of the Bean model. The B(r) profiles for applied fields increasing from H = 0 to $2H_p$, back down to H = 0, and finally to negative fields are shown in Figures APP-A4(a) through APP-A4(i) with the corresponding positions on the M(H) curve identified. The effects of lowering the applied field after raising it to $H = 2\ H_p$ are shown in Figures APP-A4(e) through APP-A4(i). At the sample's surface the field inside the superconductor will match the field outside, while $\pm J_c$ continues to flow in the sample. For the B(r) profile to match the applied field at the surface, the profile must reverse slope near the surface and it follows that the depth of this profile-reversal increases as the applied field decreases. This continues until the reversal of the profile reaches the center (on the symmetry axis) after which a further decrease in the applied field does not change the shape of the profile, although B continues to decrease inside the sample. When the applied field is reduced to zero this B(r) profile remains [see Figure APP-A4(h)]. This final state is known as the remanent critical state.

A magnetometer measures the magnetic moment of the entire sample, and from the magnetic moment, one can determine the magnetization of the sample. Magnetization is usually reported as the magnetic moment divided by the sample size, usually its mass or volume, however, these are just two of the ways magnetization value may be reported. The applied field is generally regarded as the magnetic field generated by the magnet coil and is unchanged inside the sample. Since $B = H + 4\pi M$, M is just the difference between B and H. Thus, in the plots of Figure APP-A4, M is proportional to the area between B(r) and a line corresponding to the applied field H. When the area enclosed by B(r) is above the line corresponding to H, it follows that M will be positive in sign, and when the area is below H, M will be negative. During the reversal

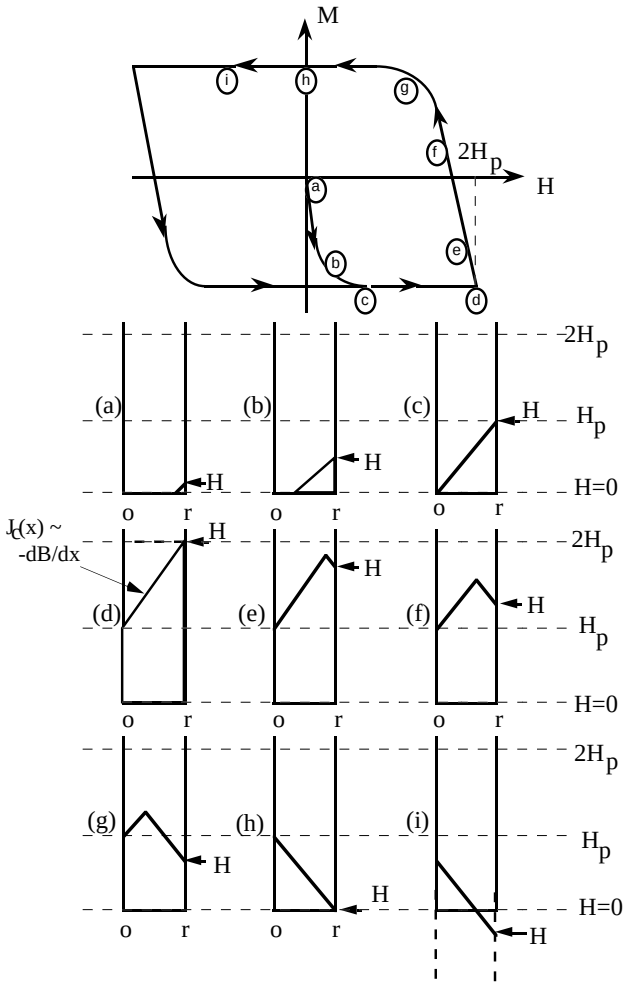

Figure APP-A4. M(H) curve for a long cylindrical sample of a strong pinning type-II superconductor in a parallel magnetic field for which the simplest version of the Bean model applies. The plots in (a) through (i) show the position dependence of the flux density B(r) as the applied field increases from zero to twice the penetration field, H_p, then down to negative applied fields. B(r) profiles at various positions on the M(H) curve are identified.

of the field profile on decreasing H, there will be regions both above and below the line corresponding to H. The sum of the areas, taking areas above H to be negative and those below H to be positive, will determine the sign of M. (Note that the plots in APP-A4 are cross sectional profiles and that the total magnetization will actually correspond to a volume rather than an area.)

The shape of the M(H) loop for a strong pinning superconductor can be accounted for by using the Bean model to follow the area between B and H through a hysteresis loop. When the sample is cooled below T_c in zero applied field (H = 0) the magnetic moment should be equal to zero. In the Bean model it is generally assumed

that $H_{c1} = 0$. Flux penetrates into the superconductor as H increases producing a linear B(r) dependence. Since the difference between the B(r) curve and the applied field is proportional to the magnetization, the magnitude of the magnetization increases as H increases. However, the M magnitude increases by a smaller and smaller percentage as more flux penetrates until the field fully penetrates the sample, at which point the M-magnitude no longer increases with H. Upon decreasing H, the B(r) profile reverses direction near the surface. Since B is going to have only one value at any point in the sample, this reversal exists to the depth where the B(r) curves meet. The reversal point continues to move deeper into the sample as H is decreased until it reaches the center of the sample, after which the profile remains the same down to H = 0. If the applied field is raised to at least twice H_p, the sample will attain the remanent critical state when the applied field is reduced to zero.

Appendix B: The MPMS Measurement And Data Analysis

1. The MPMS Measurement

The MPMS measures the local changes in magnetic flux density produced by a sample as it moves through the MPMS superconducting detection coils. The detection coils are located at the midpoint of a superconducting solenoid (normally referred to as the superconducting magnet) which can apply a DC magnetic field to the sample as specified by the user. The detection coils are connected to the input of a Superconducting QUantum Interference Device (SQUID) located in a magnetic shield some distance below the magnet and detection coils. In this configuration the detection coils are part of the superconducting input circuit of the SQUID, so that changes in the magnetic flux in the detection coils (caused by the sample moving through the coils) produce corresponding changes in the current flowing in the superconducting input current, which is detected by the SQUID. The general design of the system is shown in Figure APP-B1

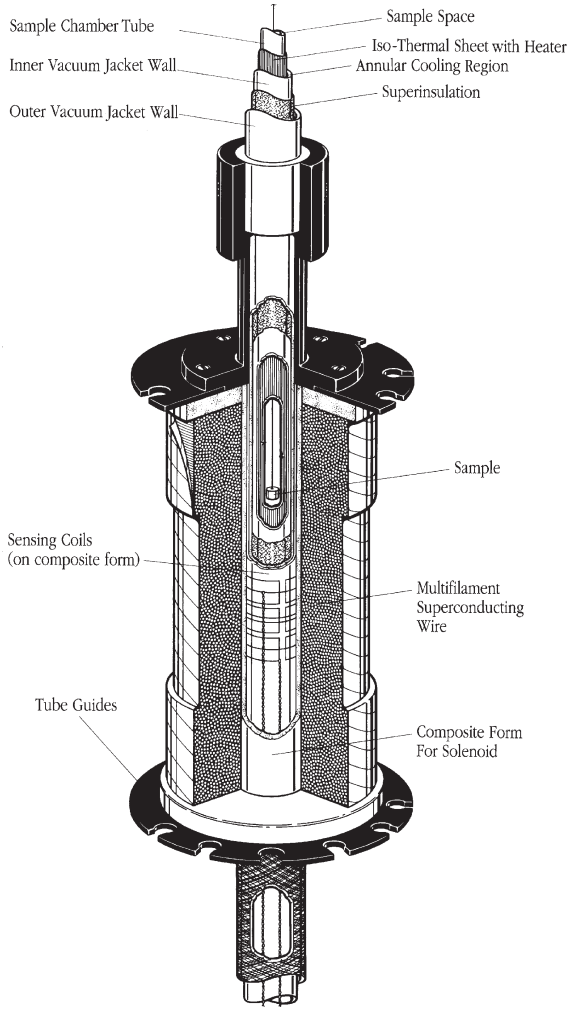

Figure APP-B1(a). The sample chamber, which extends through the center of the coils, is thermally isolated so the detection coils and magnet can remain at 4.2 K. Measurements are made by monitoring the SQUID output while moving the sample upward through the coils.

The detection coil system is wound from a single piece of superconducting wire in the form of three counterwound coils configured as a second-order (second-derivative) gradiometer. In this geometry, shown in Figure APP-B1(b), the upper coil is a single turn wound clockwise, the center coil comprises two turns wound counterclockwise, and the bottom coil is a single turn wound clockwise. The coils have a 2.02 cm diameter, and the total length of the coil system is 3.04 cm. The coils are positioned at the center of the superconducting magnet outside the sample chamber such that the magnetic field from the sample couples inductively to the coils as the sample moves through them. The second-order gradiometer configuration rejects noise caused by fluctuations of the large magnetic field of the superconducting magnet, and also reduces noise from nearby magnetic objects in the surrounding environment.

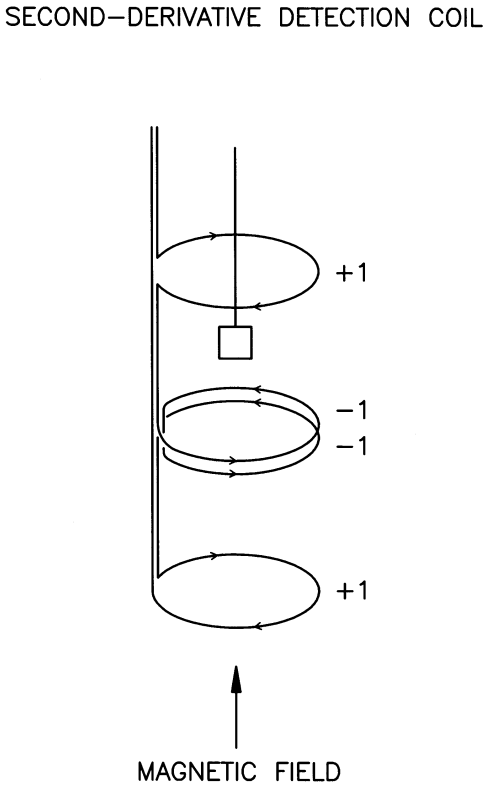

Figure APP-B1(b). The MPMS superconducting detection coils, located at the center of the MPMS superconducting magnet, are wound in a second-derivative configuration.

The MPMS determines the magnetic moment of a sample by measuring the output voltage of the SQUID detection system as the sample moves through the coil. Since changes in the output voltage of the SQUID are directly proportional to changes in the total magnetic flux in the SQUID's input circuit, transporting a point-dipole sample along the z-axis of the detection coil system produces the position-dependent output signal, V(z), shown in Figure APP-B2(a). In practice, a measurement is performed by recording the output voltage of the SQUID sensor at a number of discrete, equally spaced positions as the sample is drawn upward through the detection coils. To insure that the mechanical motion of the sample transport mechanism does not cause vibrational noise in the SQUID detection system, the measurements are performed by recording the SQUID output while the sample is held stationary at a series of points along the scan length.

A set of voltage readings from the SQUID detector, with the sample positioned at a series of equally spaced points along the scan length, comprise one complete measurement, which we refer to as a single "scan". The number of points to be read during each scan can be selected by the user; we have used 40 points for the data shown in this report. For more general measurements we recommend using 16 points when one is measuring samples which have large moments, and increasing the number of points to 32 for smaller signals. This range of values is a compromise between the need for greater averaging of small signals and the simultaneous need to stay above the low-frequency noise regime. After each scan has been completed, a mathematical algorithm is used to compute the magnetic moment of the sample from the raw data.

2. Data Analysis

All of the analyses discussed in this report were performed using the Linear Regression algorithm to fit a theoretical curve to the raw data, as shown in Figure APP-B2(a). When using this particular algorithm, the calculation also computes a regression factor, which falls within the range of 0 to 1, to indicate the quality of the fit between the theoretical curve and the raw data. (A value of 1.0 means that every point fell exactly on the theoretical curve.) When measuring a sample having a very small magnetic moment, multiple scans can be averaged together to compute an average value for the moment and a standard deviation for the set of measurements.

As discussed in the body of this report, effects which arise from the non-uniformity of the dc magnetic field can produce a magnetic response which is inconsistent with the regression algorithms used to fit the raw data points. The curve shown in Figure APP-B2(a) is the theoretical curve for a sample which behaves as a simple point-dipole moving along the axis of the detection coil system. For a real sample, the ideal curve will precisely fit the data only when: 1) the sample is positioned on the longitudinal axis of the coil system, 2) the linear dimensions of the sample are much smaller than the characteristic dimensions of the detection coils, 3) the magnetic moment of the sample does not change with position over the entire length of the scan, and 4) the sample is uniformly magnetized over its entire volume, When these conditions are met, the magnetic moment, m, of a sample can be accurately determined using the analysis methods provided

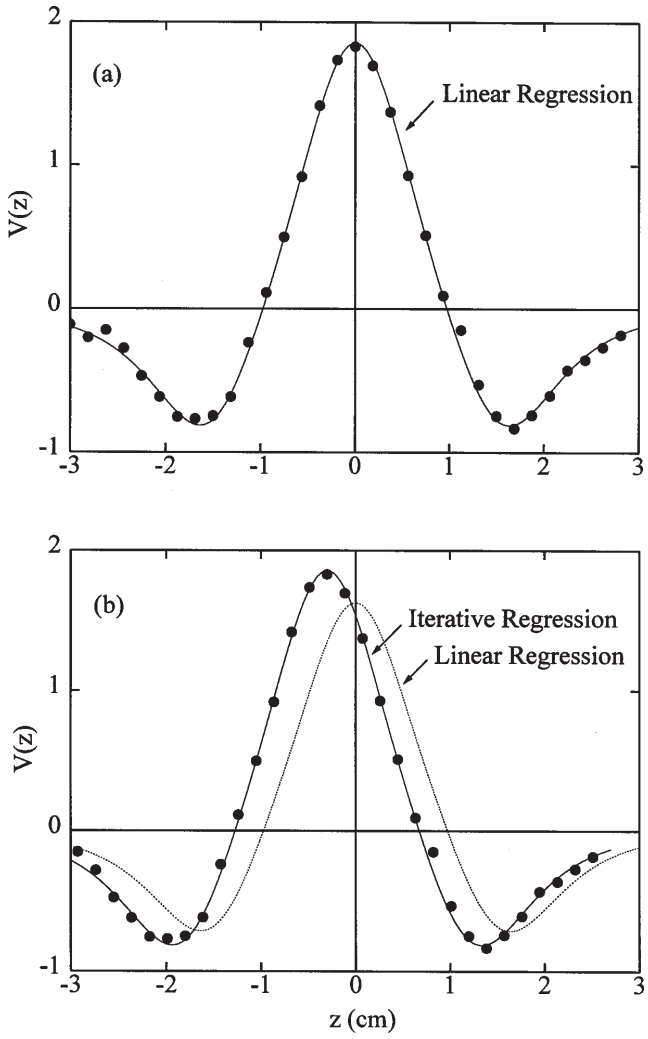

Figure APP-B2. The regression algorithms compute the magnetic moment by fitting a theoretical curve to the raw data points with the amplitude being used as the fitting parameter. The Linear Regression algorithm assumes that the data are perfectly centered along the scan length as in (a), while the Iterative Regression fit, shown by the solid line in (b) can correctly fit data which are not centered. The dashed line in (b) shows the Linear Regression fit for off center data.

with the instrument, but when making measurements on real physical samples both the position and shape of the sample can have subtle effects on the calculated magnetic moment.

The first two items, which arise from the small geometry of the detection coils used in the MPMS, essentially cause the absolute calibration of the instrument to change slightly as a function of radial position and sample volume. The effect due to the radial position of the sample is easily eliminated by using a sample holder which keeps the sample positioned close to the centerline of the sample chamber. Similarly, effects due to the size and shape of the sample can be easily corrected by a simple multiplicative factor which effectively adjusts the absolute calibration of the instrument to compensate for the shape and volume of the sample. The origin of these two effects and their correction is described more fully in Section 4 of this appendix, which discusses the calibration of the MPMS system.

Item (3), the variation of the magnetic moment of the sample as a function of position, which is the main topic of this report, is an inherent problem in any magnetometer in which the sample physically moves from one location to another during the measurement. It is also worth noting that even if one arranges to move the sample over very small distances (of the order of 0.5 mm), small variations in the magnetic field can still produce dramatic effects when measuring some types of samples, such as strong-pinning superconductors. Finally, Item (4) represents a problem which is inherent to the nature of the sample being measured. Since there is no a priori reason to assume a particular distribution for the magnetization in a nonuniformly magnetized sample, there is no general purpose theoretical model which would be suitable for analyzing such data. For this situation, however, the raw voltage data from the SQUID is available to the user when he selects the "All Scans" data file. This option allows the user to store all of the raw SQUID readings from the measurement, then use his own theoretical model to fit the raw data and perform subsequent analysis

When measuring reasonably well-behaved samples, the MPMS software provides three different mathematical algorithms for computing the magnetic moment of the sample. All three algorithms assume that the currents induced in the detection coils are those associated with the movement of a point-source magnetic dipole through a second-order gradiometer detection coil, and all three can produce errors when the raw data deviate significantly from the ideal point-dipole signal. The three analysis algorithms, which are selected in the MPMS "Set Parameters" menu, are denoted as "Full Scan", "Linear Regression", and "Iterative Regression".

2.1 The Full Scan Algorithm

The Full Scan algorithm effectively integrates the total area under the voltage-position curve, V(z), by computing the square root of the sum of the squares of the data points, normalized by the total number of data points in the scan. This algorithm was originally developed for the MPMS because it is less sensitive to changes in sample volume than the regression algorithms, but it requires a relatively long scan length (5 cm or more) to provide an accurate measurement of the absolute moment of the sample. When using the Full Scan algorithm, the magnetic moment is computed using the equation:

$$m = C \sqrt{\Delta z \sum_{i=1}^{n} V_i^2}$$

where $\Delta z = L/(n-1)$, L is the scan length, n is the number of data points in the scan, V_i is the voltage reading at the i-th point, and C is a calibration factor that includes the current-to-voltage ratio of the SQUID as well as the voltage-to-moment conversion factor for the Full Scan algorithm. The factor Δz, which is the distance between data points, normalizes the calculation for both changes in the scan length and the number of data points collected. However, measurements made with a different scan length and/or a different number of data points will give slightly different values for the absolute value of the magnetic moment.

This algorithm also has a significant limitation when used to measure very small magnetic moments. Since noise in the system always adds to the moment, the algorithm can never give a value of zero when there is any noise in the measurement. Hence, the smallest measurable moment can be severely limited by the background noise from the magnet, and there is no effective way to improve the measurement by additional averaging.

2.2 The Linear Regression Algorithm

The Linear Regression algorithm computes a least-squares fit of the theoretical voltage-position curve to the measured data set, using the amplitude of the magnetic moment as its free parameter. The algorithm assumes that the center peak of the voltage-position curve, V(z), is located precisely at the center of the measurement scan. When the sample is properly centered in the pickup coils, the central peak of the three-peaked response curve will be equidistant from both ends of the data set, as shown in Figure APP-B2(a). For the second-derivative detection coils employed in the MPMS, one can easily calculate the theoretical curve, V(z), for the general condition in which

the magnetic moment of the sample, m(z), varies with position. For this case, the output signal, V(z), is given by the following expression:

$$V(z) = \frac{-a^2 m(z)}{2}\left[\frac{1}{\{(z+d)^2+a^2\}^{\frac{3}{2}}} - \frac{1}{\{(z+b)^2+a^2\}^{\frac{3}{2}}} - \frac{1}{\{(z-b)^2+a^2\}^{\frac{3}{2}}} - \frac{1}{\{(z-d)^2+a^2\}^{\frac{3}{2}}}\right]$$

where all the coils have the same radius, a, and the four coils are positioned at z = -d, z = -b, z = b, and z = d. The origin of this coordinate system is at the center of the coil set, and the z axis lies along the axis of the coils.

In the ideal case, one assumes that the sample moves in a perfectly uniform magnetic field so the magnetic moment of the sample is constant as the sample moves through the detection coils. In this case, the position-dependent magnetic moment, m(z), in the above equation is just a constant, m, and one can easily compute the theoretical curve which is shown in Figure APP-B2(a). When the Linear Regression algorithm is used to compute the magnetic moment of the sample, the theoretical equation given above is fit to the set of position-voltage readings using a least-squares calculation with the magnetic moment, m, as its free parameter. The value of m which minimizes the least-squares calculation is then reported as the magnetic moment of the sample.

Since the Linear Regression algorithm assumes that the scan is accurately centered with respect to the detection coils, the magnetic moment reported for a scan during which the sample is not properly centered will be incorrect, with an increasing error as the misalignment increases. From Figure APP-B2(b), in which the dashed line shows a typical Linear Regression fit to a set of data which are off center by 3 mm, it is clear that the calculated magnetic moment (as indicated by the amplitude of the theoretical curve) will be too small by a significant amount. From this example, it is also clear that, when using the Linear Regression algorithm, the scan must be properly centered in the detection coils to obtain an accurate value for the magnetic moment of the sample.

However, carefully centering the sample at the beginning of a series of measurements will not guarantee accurate centering during the entire measurement sequence. Because the temperature range of the MPMS is so large, thermal expansion and contraction in the sample rod on which the sample is mounted causes the sample position to change when measurements are made over large temperature range. Consequently, a sample which has been properly centered with the sample chamber at room temperature will about 2 mm above center when the MPMS system cools down to its lowest temperature. (The total vertical displacement of the sample over the temperature range of 2 K to 400 K is approximately 3 mm.)

The present MPMS software system allows the user to resolve this problem in either of two ways. First, as discussed below, the Iterative Regression algorithm can actually compute the position of the sample by allowing the theoretical curve to move along the direction of the sample motion to obtain a better fit to the data points. Alternatively, one can use the automatic "Sample Tracking" feature of the MPMS which automatically adjusts the position of the sample as the temperature changes to keep the sample properly centered to within about 0.3 mm over the entire temperature range. When using the Sample Tracking feature, however, it is essential that the user accurately center the sample at the beginning of the measurement sequence, since the Sample Tracking algorithm assumes that the sample was correctly positioned at the beginning of the sequence.

The Linear Regression algorithm is the most reliable calculation if one is measuring a sample which has a very small magnetic moment. Since this algorithm can inherently produce a value of zero (unlike the Full Scan algorithm), it can more effectively average the noise when measuring small samples. Furthermore, its most significant limitation, the errors introduced by changes in the sample position, has been virtually eliminated by the Sample Tracking capability of the MPMS system, allowing the Linear Regression algorithm to provide reliable data over the full temperature range of the MPMS. Because of the reliability of the Linear Regression algorithm and the Sample Tracking feature, this is now the recommended analysis method.

2.3 The Iterative Regression Algorithm

The Iterative Regression algorithm, which can report the correct value for the magnetic moment even when the scan is not properly centered, is designed to compensate for centering errors as large as 1 cm. This theoretical model uses the same constant-dipole equation as the Linear Regression calculation, but allows the position of the theoretical curve to vary along the axis of the detection coils.

Mathematically this is achieved by substituting $z' + s$ for z in the above equation, where the variable, s, now becomes a second free parameter which can be varied to improve the least squares fit to the data. Since the variable s appears in the equation as a displacement along the z-axis, changing the value of s is equivalent to shifting the position of the theoretical curve along the axis of the coil system.

The resulting equation now has two variables and is nonlinear in s, so one cannot simply compute both m and s from the Linear Regression algorithm. To find the optimum values for both m and s, the Iterative Regression algorithm first computes a standard Linear Regression calculation taking the value of s to be zero. Then, based on a derivative calculation, a new value of s is selected and the linear regression calculation is repeated. By comparing the regression factors on subsequent calculations (which indicates the accuracy of the regression fit) , the algorithm can determine the values for s and m which minimize the least-squares calculation, and the resulting value of m is reported as the magnetic moment of the sample. A typical theoretical fit computed by the Iterative Regression algorithm for a scan which is 3 mm off center is shown by the solid line in Figure APP-B2(b).

The Iterative Regression algorithm was developed to compensate for incorrect sample position, and the algorithm works extremely well for measurements which have a large signal-to-noise ratio so the peaks are well defined. However, when the sample moment is very small the iterative process can be confused by low frequency noise in the measurement. More specifically, when the peaks in the sample signal are of approximately the same size as the low frequency magnetic noise from the superconducting magnet, the iterative regression algorithm will sometimes fit the analytical curve to features in the data which are characteristic of the noise in the system rather than the data. Also, the iterative process may fail to converge. This condition is indicated by a computed sample position which is more than 1cm off center, well beyond the maximum possible position for a properly centered sample. When this condition occurs, the system reverts to using the Linear Regression algorithm.

It is clear from the above discussion that each analysis algorithm has both strengths and weaknesses. However, as we have consistently emphasized in this report, it is important to understand that all of the algorithms can give incorrect values for the magnetic moment when one is measuring samples which are not uniformly magnetized, or when the magnetic moment of the sample changes with position along the scan length.

3. The MPMS Superconducting Magnet

The MPMS system employs a superconducting magnet and a precision current supply to generate the large, highly stable dc magnetic fields required for the measurement system. When a large stable magnetic field (> 2 tesla) is needed over a modest volume, a superconducting magnet is normally chosen, but there are numerous issues which must be taken into consideration when using a superconducting magnet. For example, after the MPMS superconducting magnet has been charged to fields greater than about 200 G, magnetic field lines will become trapped in the magnet's superconducting windings, so that when the magnet current is set back to zero, the actual measurable magnetic field at the center of the magnet may be as large as 40 G to 50 G. This so-called "trapped flux" is characteristic of all superconducting magnets, although this "remanent field" which is left in the magnet when the magnet transport current is discharged to zero will depend strongly on the size and specific design of the magnet.

While the remanent field in the various MPMS magnets is small compared to the maximum available field, the remanent field can still introduce a substantial error when performing measurements in the MPMS at very low fields. In this case it is important to determine and account for the effect of the remanent field in the magnet. One important effect discussed in this report is the variation of the remanent field as a function of vertical position (z-dependence) over which the sample moves during a measurement. The MPMS system provides several mechanisms for reducing the remanent field and increasing its uniformity when the user needs to perform measurements at low magnetic fields.

Another important feature of superconducting magnets, particularly when employed in a high-sensitivity measurement system such as the MPMS, is that after the magnetic field has been changed, the field in the magnet will relax logarithmically in time. This process, which occurs because the magnetic flux creeps across the magnet's superconducting windings, proceeds even after the magnet has been placed in a persistent condition (with the persistent-current switch in its superconducting state, and the magnet power supply turned off). While the relaxation effect is relatively small compared to the maximum available field, under some conditions — particularly when measuring near the limit of the MPMS's sensitivity after a large change in the value of the field — this relaxation can generate a signal in the high-sensitivity SQUID detection system which is many times larger than the signal to be measured.

Because the time constant for the magnet relaxation (typically several minutes) is quite long compared to the length

of an single sample measurement (about 10 seconds), the background relaxation can usually be treated as a linear background signal, which is automatically eliminated by the data analysis routines. However, if a very small signal is to be measured immediately after a magnetic field change, the background drift can be so large that the 16-bit dynamic range of the MPMS digitizing system may not be able to achieve the resolution needed to measure the signal in the presence of the relaxing background. To accommodate this situation, the MPMS system provides a "Pause" function which allows the user to specify the length of time to wait after a magnetic field change before beginning the next measurement.

The MPMS system provides four different methods for changing the magnetic field in the system, allowing the user to tailor the magnet control for particular measurements. The "No-Overshoot", "Oscillate", and "Hysteresis" modes are useful for routine changes between arbitrary starting and ending values, while the magnet reset option provides a special method for eliminating trapped flux from the superconducting MPMS magnet. When the No-Overshoot method is used, the magnetic field is changed monotonically from the initial field to the desired field setting. At the beginning of the field change, the field is ramped quickly, but as the field approaches the requested value, the field changes much more slowly to avoid overshooting the target value. When using the Oscillate method, the magnetic field alternately overshoots and undershoots the requested value with the amplitude of the overshoot and undershoot decreasing on each cycle. This process minimizes the relaxation in the superconducting magnet following the field change, but is inappropriate when measuring samples which display magnetic hysteresis effects. When changing the magnetic field using the No-Overshoot and Oscillate modes, the magnet is put into a persistent condition after the final field is reached, with the magnet switch heater and power supply turned off while measurements are being performed.

In the Hysteresis mode, the magnet is charged directly to the final field, and measurements are performed while the magnet current is being maintained by the power supply (with the magnet switch heater turned on). This allows measurements to be made at sequential field settings much more rapidly than normal, but the sensitivity of such measurements is substantially reduced due to the increased magnetic noise from the magnet supply current when operating in this mode. This measurement is most suitable for measuring the hysteresis curves of samples which have fairly large magnetic moments.

The "Magnet Reset" option provides a mechanism by which the user can remove magnetic flux trapped in the superconducting magnet windings after the magnet has been charged to high fields. In the 55-kG (5.5-tesla) MPMS magnets, the Magnet Reset operation comprises a controlled quench in which part of the magnet is driven normal while the magnet is sustaining a persistent current. In the 10-kG (1-tesla) MPMS magnet, and the high uniformity model-5S 50-kG (5-tesla) and model-7S 70-kG (7-tesla) magnets, the magnet heater is capable of driving the entire magnet normal without requiring that the magnet be quenched.

When the reset operation is initiated to induce a quench of the superconducting magnet, a portion of the superconducting windings is driven normal (non-superconducting) and becomes resistive. Resistive losses in this segment of the magnet then generate heat which causes additional parts of the magnet to become resistive, and the quench becomes a runaway situation in which all of the superconducting magnet windings are eventually driven normal. When this occurs, the persistent current in the magnet quickly decays to zero, and any magnetic flux previously trapped in the superconducting windings is released. The magnet reset option leaves the magnetic field in the MPMS magnet in a state similar to that observed when the magnet has just been cooled down from room temperature and has not yet been charged to fields above approximately 200 G. The field remaining in the magnet following a quench will typically be approximately the size of the Earth's field, about 0.5 G, although this value may vary if the MPMS system has an external magnetic shield around the dewar.

To provide the capability for the user to make measurements in very low magnetic fields (less than 10 milligauss), the MPMS systems offer the "Low-Field Option" which employs a flux-gate magnetometer to measure and null the field left in the magnet after a quench process has been completed. The low-field option, which is available on MPMS systems having 10-kG (1-tesla) magnets and the high-uniformity model-5S 50-kG (5-tesla) magnet, automatically measures the field at the center of the magnet, then adjusts the current in the magnet to null the remaining field to less than 0.005 G (0.050 G for the Model 5S magnet). The user may also measure the field profile in the magnet along its vertical axis by scanning the flux-gate magnetometer along the axis of the magnet.

4. MPMS System Calibration

All of the data analysis routines in the MPMS report the magnetic moment of the sample in cgs or electromagnetic units. To insure that the reported values accurately represent the absolute magnetic moment of the sample, the instrument calibration at the factory employs a sample of known susceptibility in the form of a right circular cyl-

inder having a dimension of 2.5 mm for both diameter and height. If the shape of your sample deviates significantly from a right circular cylinder, or if the sample is much larger than the standard calibration sample, you may wish to recalibrate your measurements using a reference sample having the same shape and dimensions as the experimental sample.

As noted in Section 2 above, the absolute calibration of the instrument changes slightly with the size and shape of the sample and also with the radial position of the sample in the sample chamber. These effects result from the small geometry of the MPMS detection coils, which was originally chosen for the multiple benefits it provides. The most important benefits of the small geometry are: (1) it allows a complete scan to be made over a small distance, minimizing the distance which the sample must move during the measurement, (2) it improves the rejection of noise from the dc magnetic field, (3) it optimizes the magnetic coupling between the coils and the sample, allowing measurements to be made on samples which have extremely small volumes, and (4) it allows the use of a much smaller magnet, minimizing cost, allowing faster charging rates, and reducing helium loss while the magnet is charging.

However, detection coils which use a small geometry are more sensitive to the radial position of the sample. To be specific, measurements in which a sample is located at the outer edge of the sample chamber will give a somewhat different result for the magnetic moment, than a sample which is located precisely on the centerline of the coil system. This effect, which results from the r-cubed nature of the dipole field, means that a sample which is

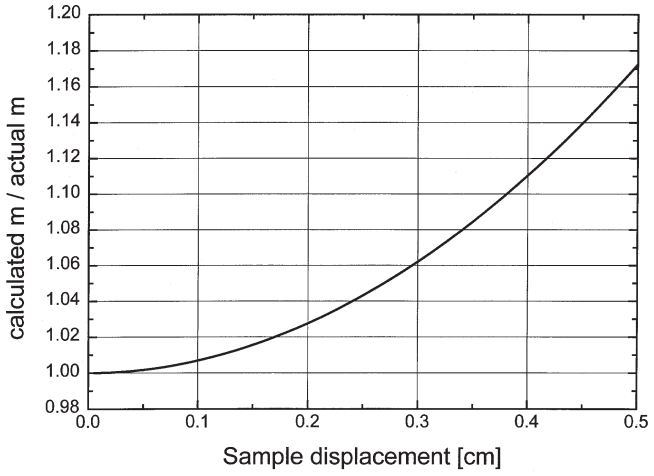

Figure APP-B3. The variation of the measured magnetic moment as a function of radial position for measurements using a second-derivative coil system. This dependence occurs because the mutual inductance between the sample and the detection coils changes with the radial position of the sample.

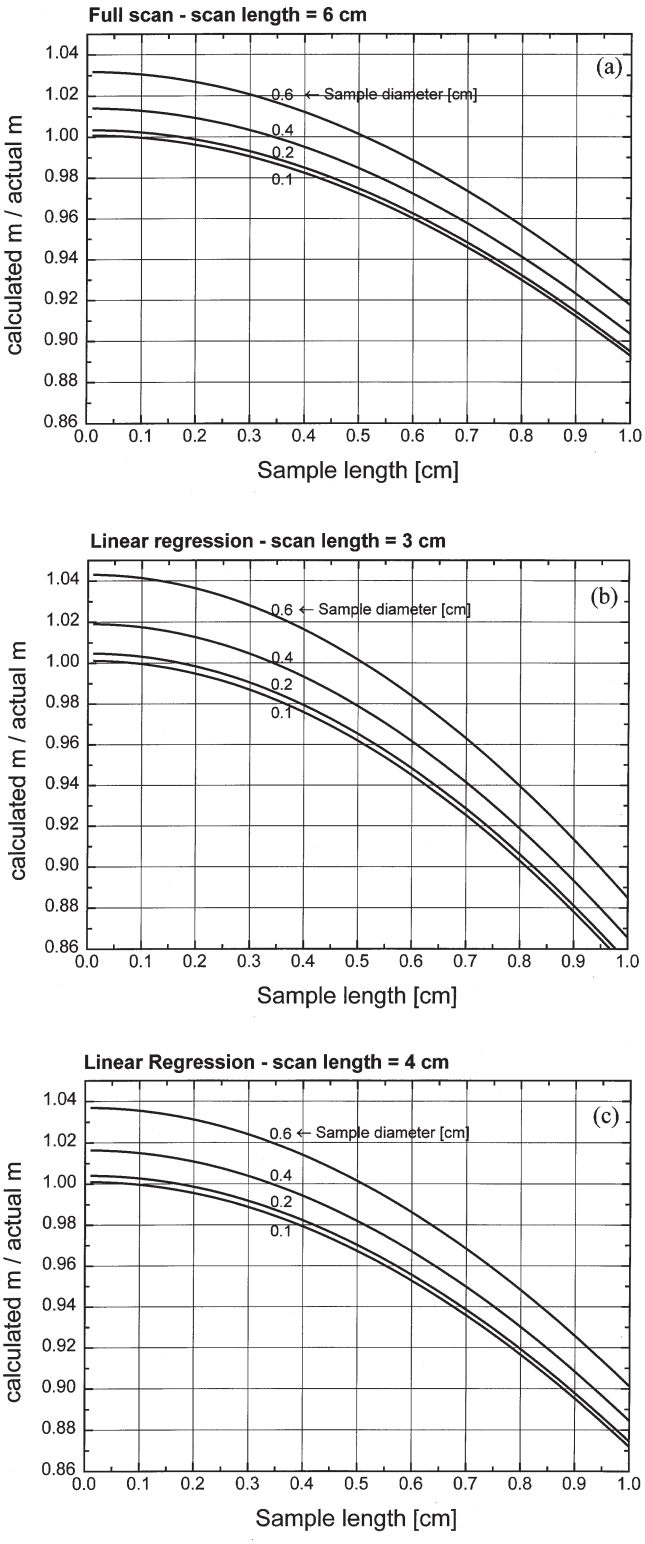

Figure APP-B4. Variation of the measured magnetic moment as a function of sample length and diameter for three combinations of measurement and analysis selections: (a) Full Scan algorithm with a 6 cm scan, (b) Linear Regression using a 3 cm scan, and (c) Linear Regression using a 4 cm scan. Linear Regression corrections also apply to Iterative Regression algorithm.

off center will produce a greater net flux in the detection coils than a sample located exactly on the longitudinal axis of the coil system. Figure APP-B3 shows the variation of the moment as a function of radial position for the MPMS for a point-dipole sample. This effect can be rather large (over 10% at the wall of the sample chamber), but it can be essentially eliminated by using a sample holder that keeps the sample reasonably close to the centerline of the sample chamber.

The nonlinearity associated with the size and shape of the sample also arises from the radial dependence of the coil system. By the same argument, if the sample to be measured has a large diameter, the outermost parts of the sample will produce a larger relative contribution to the signal than the center-most portion of the sample. A similar argument applies to long samples. Since the coils are spaced closely together (with a distance of only 1.52 cm between adjacent coils), the end of a long sample will be entering the effective measuring volume of one coil before the opposite end of the sample has left the measuring volume of the adjacent coil. Because of these two effects, the calculated magnetic moment will not increase exactly as expected with either increasing length or increasing diameter.

Figure APP-B4(a) shows the calculated correction as a function of sample length for the Full Scan algorithm using a 6 cm scan length. Figures APP-B4(b) and APP-B4(c) show the results of similar calculations for the Linear Regression algorithm for a 3 cm scan length and 4 cm scan length respectively. (The correction factors shown in Figure APP-B4(b) and APP-B4(c) can also be used for the Iterative Regression algorithm.) From these figures one can see that long needle-like samples will give values that are several percent smaller than expected, while thin disk-like samples will give values that can be a few percent too large. The correction for intermediate sample shapes can also be determined from these figures.

This effect is strictly related to the shape and volume of the sample, and the appropriate multiplicative factor to correct the reported values of magnetic moment can be determined from the graphs shown in Figure APP-B4. Please note that these calculations do NOT include any corrections for the geometrical demagnetizing factor associated with different shapes. Corrections for the proper demagnetizing factor must be included if one wishes to calculate a theoretical value for the magnetic moment for any specific sample shape.

This volumetric or shape effect can also be corrected by adjusting the instrument calibration factor for a specific shape by recalibrating the MPMS using a piece of material of the desired size and shape but having known magnetic properties. When an unknown sample of similar size and shape is measured, the system will then report the correct absolute values of magnetic moment. We have found that Standardized Pd wire from the National Institutes of Standards and Technology (NIST) is especially useful for making reference samples in a variety of geometries.

One final note which may be of interest to the user concerns the palladium reference samples supplied with the Quantum Design MPMS. These samples are made from 99.995%-purity palladium material which has been fully characterized through a series of measurements in an MPMS system. The residual iron content in the material used for the reference samples was specified by the manufacturer to be 8 parts per million (ppm), but an independent assay reported a value of 24 ppm iron content. (Cobalt and Nickel content were reported to be 0.1 ppm.) Although the iron content of the palladium is small, it is still large enough to produce a noticeable saturable magnetic moment when measuring this material in low magnetic fields. Consequently, when using one of these reference samples to check the calibration of an MPMS, one should account for the presence of the iron impurities to achieve the best value of the instrument calibration.